

# QUARKONIUM AT FINITE TEMPERATURE

Alexei Bazavov

*Department of Physics, University of Arizona, Tucson, AZ 85721, USA*

Péter Petreczky

*RIKEN-BNL Research Center and Physics Department,  
Brookhaven National Laboratory, Upton NY 11973, USA*

Alexander Velytsky\*

*Enrico Fermi Institute, University of Chicago, 5640 S. Ellis Ave.,  
Chicago, IL 60637, USA*

*and*

*HEP Division and Physics Division, Argonne National Laboratory,  
9700 Cass Ave., Argonne, IL 60439, USA*

We discuss properties of heavy quarkonium states at high temperatures based on lattice QCD and potential models. We review recent progress made in lattice calculations of spatial static quark anti-quark correlators as well as quarkonium correlators in Euclidean time. Recent developments in effective field theory approach and potential models are also discussed.

## 1. Introduction

There was considerable interest in the properties and the fate of heavy quarkonium states at finite temperature since the famous conjecture by Matsui and Satz [1]. It has been argued that color screening in medium will lead to quarkonium dissociation above deconfinement, which in turn can signal quark gluon plasma formation in heavy ion collisions. The basic assumption behind the conjecture by Matsui and Satz was the fact that medium effects can be understood in terms of a temperature dependent heavy quark potential. Color screening makes the potential exponentially suppressed at distances larger than the Debye radius and it therefore cannot bind the heavy quark and anti-quark once the temperature is sufficiently high. Based on this idea potential models at finite temperature with different temperature dependent potentials have been used over the last two decades to study quarkonium properties at finite temperature (see Ref. [2] for a recent review). It was not until recently that effective field theory approach, the so-called thermal pNRQCD, has been developed to justify the use of potential models at finite temperature [3]. This

\*current address: Physics Department, Brookhaven National Laboratory, Upton NY 11973, USA

approach, however, is based on the weak coupling techniques and will be discussed in the next section. To understand the non-perturbative aspects of color screening lattice calculations of the spatial correlation functions of static quarks are needed. Recently a lot of progress has been made in this direction which will be the topic of section 4. To prepare the reader for this in section 3 we review the basics of lattice gauge theory.

In principle it is possible to study the problem of quarkonium dissolution without any use of potential models. In-medium properties of different quarkonium states and/or their dissolution are encoded in spectral functions. Spectral functions are related to Euclidean meson correlation functions which can be calculated on the lattice. Reconstruction of the spectral functions from the lattice meson correlators turns out to be very difficult, and despite several attempts its outcome still remains inconclusive. One remarkable feature of the studies of the lattice meson correlators is their small temperature dependence despite the expected color screening. This seems to be puzzling. We will discuss the possible resolution of this puzzle in section 6, while the current status of the lattice calculations of the Euclidean correlators and the corresponding meson spectral functions will be presented in section 5. The summary and outlook will be given in section 7.

## 2. pNRQCD at finite temperature

There are different scales in the heavy quark bound state problem related to the heavy quark mass  $m$ , the inverse size  $\sim mv$  and the binding energy  $mv^2$ . Here  $v$  is the typical heavy quark velocity in the bound state and is considered to be a small parameter. Therefore it is possible to derive a sequence of effective field theories using this separation of scales (see Refs. [4, 5] for recent reviews). Integrating out modes at the highest energy scale  $\sim m$  leads to an effective field theory called non-relativistic QCD or NRQCD, where the pair creation of heavy quarks is suppressed by powers of the inverse mass and the heavy quarks are described by non-relativistic Pauli spinors [6]. At the next step, when the large scale related to the inverse size is integrated out, the potential NRQCD or pNRQCD appears. In this effective theory the dynamical fields include the singlet  $S(r, R)$  and octet  $O(r, R)$  fields corresponding to the heavy quark anti-quark pair in singlet and octet states respectively, as well as light quarks and gluon fields at the lowest scale  $\sim mv^2$ . The Lagrangian of this effective field theory has the form

$$\begin{aligned} \mathcal{L} = & -\frac{1}{4}F_{\mu\nu}^a F^{a\mu\nu} + \sum_{i=1}^{n_f} \bar{q}_i i \not{D} q_i + \int d^3r \text{Tr} \left\{ S^\dagger \left[ i\partial_0 + \frac{\nabla_r^2}{m} - V_s(r) \right] S \right. \\ & \left. + O^\dagger \left[ iD_0 + \frac{\nabla_r^2}{m} - V_o(r) \right] O \right\} + V_A \text{Tr} \left\{ O^\dagger \vec{r} \cdot g \vec{E} S + S^\dagger \vec{r} \cdot g \vec{E} O \right\} \\ & + \frac{V_B}{2} \text{Tr} \left\{ O^\dagger \vec{r} \cdot g \vec{E} O + O^\dagger O \vec{r} \cdot g \vec{E} \right\} + \dots \end{aligned} \quad (1)$$

Here the dots correspond to terms which are higher order in the multipole expansion [5]. The relative distance  $r$  between the heavy quark and anti-quark plays a role of a label, the light quark and gluon fields depend only on the center-of-mass coordinate  $R$ . The singlet  $V_s(r)$  and octet  $V_o(r)$  heavy quark potentials appear as matching coefficients in the Lagrangian of the effective field theory and therefore can be rigorously defined in QCD at any order of the perturbative expansion. At leading order

$$V_s(r) = -\frac{N^2 - 1}{2N} \frac{\alpha_s}{r}, \quad V_o(r) = \frac{1}{2N} \frac{\alpha_s}{r} \quad (2)$$

and  $V_A = V_B = 1$ .

The free field equation for the singlet field is

$$\left[ i\partial_0 + \frac{\nabla_r^2}{m} - V_s(r) \right] S(r, R) = 0, \quad (3)$$

i.e. has the form of a Schrödinger equation with the potential  $V_s(r)$ . In this sense, potential models emerge from the pNRQCD. Note, however, that pNRQCD also accounts for interaction of the soft gluons which cannot be included in potential models, i.e. it can describe retardation effects.

One can generalize this approach to finite temperature. However, the presence of additional scales makes the analysis more complicated [3]. The effective Lagrangian will have the same form as above, but the matching coefficients may be temperature dependent. In the weak coupling regime there are three different thermal scales :  $T$ ,  $gT$  and  $g^2T$ . The calculations of the matching coefficients depend on the relation of these thermal scales to the heavy quark bound state scales [3]. To simplify the analysis the static approximation has been used, in which case the scale  $mv$  is replaced by the inverse distance  $1/r$  between the static quark and anti-quark. The binding energy in the static limit becomes  $V_o - V_s \simeq N\alpha_s/(2r)$ . When the binding energy is larger than the temperature the derivation of pNRQCD proceeds in the same way as at zero temperature and there is no medium modifications of the heavy quark potential [3]. But bound state properties will be affected by the medium through interactions with ultra-soft gluons, in particular, the binding energy will be reduced and a finite thermal width will appear due to medium induced singlet-octet transitions arising from the dipole interactions in the pNRQCD Lagrangian [3] (c.f. Eq. (1)). When the binding energy is smaller than one of the thermal scales the singlet and octet potential will be temperature dependent and will acquire an imaginary part [3]. The imaginary part of the potential arises because of the singlet-octet transitions induced by the dipole vertex as well as due to the Landau damping in the plasma, i.e. scattering of the gluons with space-like momentum off the thermal excitations in the plasma. In general, the thermal corrections to the potential go like  $(rT)^n$  and  $(m_D r)^n$  [3], where  $m_D$  denotes the Debye mass. Only for distances  $r > 1/m_D$  there is an exponential screening. In this region the singlet

potential has a simple form

$$V_s(r) = -C_F \frac{\alpha_s}{r} e^{-m_D r} + i C_F \alpha_s T \frac{2}{r m_D} \int_0^\infty dx \frac{\sin(m_D r x)}{(x^2 + 1)^2} - C_F \alpha_s (m_D + iT),$$

$$C_F = (N^2 - 1)/(2N) \quad (4)$$

The real part of the singlet potential coincides with the leading order result of the so-called singlet free energy [7]. The imaginary part of the singlet potential in this limit has been first calculated in [8]. For small distances the imaginary part vanishes, while at large distances it is twice the damping rate of a heavy quark [9]. This fact was first noted in Ref. [10] for thermal QED.

The effective field theory at finite temperature has been derived in the weak coupling regime assuming the separation of different thermal scales as well as  $\Lambda_{QCD}$ . In practice the separation of these scales is not evident and one needs lattice techniques to test the approach. Therefore section 4 will be dedicated to the study of static quarks at finite temperature on the lattice. To prepare the reader for this discussion some basics of the lattice gauge theory will be given in the next section.

### 3. Basics of lattice gauge theory

To study non-perturbative aspects of QCD we use lattice gauge theory [11]. In this formalism a field theory is defined in a gauge-invariant way on a discrete space-time domain. This serves at least two purposes: a) to provide an ultra-violet cut-off for the theory, restricting highest momentum to  $\pi/a$  ( $a$  being the lattice spacing), and b) to evaluate the path integrals in the Euclidean formulation stochastically using importance sampling.

On the lattice the fundamental degrees of freedom of a theory with local  $SU(N)$  gauge symmetry are fermion fields  $\psi_x$  that reside on the sites of the lattice and carry flavor, color and Dirac indices, which we suppress through the most of this paper, and gauge, bosonic degrees of freedom that in the form of  $SU(N)$  matrices  $U_{x,\mu}$  reside on links. Sites on a four-dimensional lattice are labeled with  $x \equiv (\vec{x}, t)$ .

The theory is defined by the partition function

$$Z = \int D U D \bar{\psi} D \psi \exp(-S) \quad (5)$$

where the action

$$S = S_g + S_f \quad (6)$$

contains gauge,  $S_g$  and fermionic,  $S_f$  parts. The latter part is bi-linear in fields and has the form

$$S_f = \bar{\psi} M \psi \quad (7)$$

where  $M$  is the fermion matrix. In the simplest formulation the lattice gauge action can be written as

$$S_g = \beta \sum_P \left( 1 - \frac{1}{N} \text{Tr} U_P \right), \quad (8)$$

where  $U_P$  is the so-called plaquette, a product of link variables along the elementary square and  $\beta = 2N/g^2$  with  $g^2$  being the bare gauge coupling. This is the Wilson gauge action [11]. The explicit form of the fermion action that is often used in lattice QCD calculations will be discussed in section 5.2.

The expectation value of an operator  $\hat{O}$  is given then by

$$\langle \hat{O} \rangle = \frac{1}{Z} \int DU D\bar{\psi} D\psi \hat{O} \exp(-S). \quad (9)$$

Integration over the fermion fields (which are Grassmann variables) can be carried out explicitly:

$$Z = \int DU \det M[U] \exp(-S_g) \equiv \int DU \exp(-S_{eff}), \quad (10)$$

where  $S_{eff} = S_g - \ln \det M[U]$  is the effective action. The fermion determinant  $\det M[U]$  describes the vacuum polarization effects due to the dynamical quarks and makes the effective action non-local in gauge variables. For this reason simulations with dynamical quarks are very resource demanding and the quenched approximation is often employed, where  $\det M[U]$  is set to 1.

To evaluate the path integral (9) stochastically, an ensemble of  $N_U$  gauge configurations, weighted with  $\exp(-S_{eff})$ , is generated using Monte Carlo or Molecular Dynamics techniques. The expectation value of the operator is then approximated by the ensemble average:

$$\langle \hat{O} \rangle \simeq \frac{1}{N_U} \sum_{i=1}^{N_U} O_i(U), \quad (11)$$

where  $O_i(U)$  is the value of the operator  $\hat{O}$ , calculated on  $i$ -th configuration. (When the operator  $\hat{O}$  depends explicitly on the quark fields extra factors of  $M^{-1}$  appear as shown for a meson correlator below.)

Consider a meson (quark anti-quark pair) operator of a general form

$$J(\vec{x}, \vec{y}; t) = \bar{\psi}(\vec{x}, t) \Gamma \mathcal{U}(\vec{x}, \vec{y}; t) \psi(\vec{y}, t), \quad (12)$$

where  $\Gamma$  determines the spin structure and  $\mathcal{U}$  is a gauge connection that corresponds to the excitations of the gluonic field. Dirac and color indices in (12) are suppressed.

The propagation of such meson from time  $t = 0$  to  $t$  is described by the correlation function

$$\begin{aligned} \langle J(\vec{x}_1, \vec{y}_1; 0) J(\vec{x}_2, \vec{y}_2; t) \rangle &= \frac{1}{Z} \int DU D\bar{\psi} D\psi \exp(-S) \\ &\times \bar{\psi}(\vec{x}_1, 0) \Gamma \mathcal{U}(\vec{x}_1, \vec{y}_1; 0) \psi(\vec{y}_1, 0) \bar{\psi}(\vec{y}_2, t) \Gamma^\dagger \mathcal{U}^\dagger(\vec{x}_2, \vec{y}_2; t) \psi(\vec{x}_2, t). \end{aligned} \quad (13)$$

Again, integration over the quark fields can be carried out resulting in

$$\begin{aligned} \langle J(\vec{x}_1, \vec{y}_1; 0) J(\vec{x}_2, \vec{y}_2; t) \rangle = & \\ & \langle \text{Tr} [M^{-1}(\vec{x}_2, t; \vec{x}_1, 0) \Gamma \mathcal{U}(\vec{x}_1, \vec{y}_1; 0) M^{-1}(\vec{y}_1, 0; \vec{y}_2, t) \Gamma^\dagger \mathcal{U}^\dagger(\vec{x}_2, \vec{y}_2; t)] \rangle \\ & - \langle \text{Tr} [M^{-1}(\vec{y}_1, 0; \vec{x}_1, 0) \Gamma \mathcal{U}(\vec{x}_1, \vec{y}_1; 0)] \rangle \\ & \times \langle \text{Tr} [M^{-1}(\vec{x}_2, t; \vec{y}_2, t) \Gamma^\dagger \mathcal{U}^\dagger(\vec{x}_2, \vec{y}_2; t)] \rangle. \end{aligned} \quad (14)$$

The inverse of the fermion matrix,  $M^{-1}$  has meaning of a fermion propagator.

Gauge transporters  $\mathcal{U}(\vec{x}, \vec{y}; t)$  can be taken as weighted sums of different paths connecting points  $\vec{x}$  and  $\vec{y}$ . By choosing paths of certain shape or combinations of different paths it is possible to achieve a better overlap of the meson operator with a given state. One of the possibilities is to construct the gauge transporters by using APE smearing [12] on spatial links: a link variable  $U_{x,\mu}$  is replaced by a weighted average of itself and a sum of the 3-link paths connecting the same sites as  $U_{x,\mu}$ :

$$U_{x,\mu} \rightarrow U'_{x,\mu} = (1 - 6c)U_{x,\mu} + c \sum_{\nu \neq \mu} U_{x,\mu} U_{x+\hat{\nu},\mu} U_{x+\hat{\mu},\nu}^\dagger. \quad (15)$$

This procedure can be applied iteratively. Then a gauge transporter  $\mathcal{U}(\vec{x}, \vec{y}; t)$ , taken as a product of smeared links, is equivalent to a weighted sum of differently shaped paths connecting the sites  $\vec{x}$  and  $\vec{y}$ .

In the following we will consider meson correlators at finite temperature. The finite temperature is introduced by compactifying the the Eucliden time direction, i.e.  $T = 1/(N_\tau a)$  with  $N_\tau$  being the number of temporal time slices. Gauge fields and fermion fields obey periodic and anti-periodic boundary conditions in the temporal direction. In the next section we consider a spinless static quark anti-quark pair,  $\Gamma = \mathbf{I}$  that can propagate only in time. In this case second term in (14) vanishes. In Sec. 5 we consider local meson operators with  $\vec{x}_i = \vec{y}_i$ ,  $i = 1, 2$  which means  $\mathcal{U}(\vec{x}, \vec{y}; t) = \mathbf{I}$ .

## 4. Correlation functions of static quarks in lattice gauge theory

### 4.1. Static meson correlators

Consider static (infinitely heavy) quarks. The position of heavy quark anti-quark pair is fixed in space and propagation happens only along the time direction. In this limit the second term on the right hand side of (14) vanishes. We are interested in a spinless state and set  $\Gamma = \mathbf{I}$  in this section. With respect to the color the meson can be in a singlet or adjoint state. These states are described by the following gauge connections

$$\mathcal{U}(\vec{x}, \vec{y}; t) = U(\vec{x}, \vec{y}; t), \quad (16)$$

$$\mathcal{U}^a(\vec{x}, \vec{y}; t) = U(\vec{x}, \vec{x}_0; t) T^a U(\vec{x}_0, \vec{y}; t), \quad (17)$$

where  $U(\vec{x}, \vec{y})$  is a spatial gauge transporter, – the product of the gauge variables along the path connecting  $\vec{x}$  and  $\vec{y}$ ,  $\vec{x}_0$  is the coordinate of the center of mass of the meson and  $T^a$  are the  $SU(N)$  group generators.

The meson operators are given then by Eq. (12) with  $\vec{x}_1 = \vec{x}_2$ ,  $\vec{y}_1 = \vec{y}_2$  for static quarks

$$J(\vec{x}, \vec{y}; t) = \bar{\psi}(\vec{x}, t) U(\vec{x}, \vec{y}; t) \psi(\vec{y}, t), \quad (18)$$

$$J^a(\vec{x}, \vec{y}; t) = \bar{\psi}(\vec{x}, t) U(\vec{x}, \vec{x}_0; t) T^a U(\vec{x}_0, \vec{y}; t) \psi(\vec{y}, t). \quad (19)$$

Substituting expressions (18) into eq. (14) and noting that for a static quark the propagator  $M^{-1}(\vec{x}, 0; \vec{x}, t) \sim L(\vec{x})$ , where the temporal Wilson line  $L(\vec{x}) = \prod_{t=0}^{N_\tau-1} U(\vec{x}, t, 0)$  with  $U(\vec{x}, t, 0)$  being the temporal links, we get for the meson correlators at  $t = 1/T$ :

$$\begin{aligned} G_1(r, T) &\equiv \frac{1}{N} \langle J(\vec{x}, \vec{y}; 0) \bar{J}(\vec{x}, \vec{y}; 1/T) \rangle \\ &= \frac{1}{N} \langle \text{Tr} [L^\dagger(\vec{x}) U(\vec{x}, \vec{y}; 0) L(\vec{y}) U^\dagger(\vec{x}, \vec{y}, 1/T)] \rangle, \end{aligned} \quad (20)$$

$$\begin{aligned} G_a(r, T) &\equiv \frac{1}{N^2 - 1} \sum_{a=1}^{N^2-1} \langle J^a(\vec{x}, \vec{y}; 0) \bar{J}^a(\vec{x}, \vec{y}; 1/T) \rangle \\ &= \frac{1}{N^2 - 1} \langle \text{Tr} L^\dagger(x) \text{Tr} L(y) \rangle \\ &\quad - \frac{1}{N(N^2 - 1)} \langle \text{Tr} [L^\dagger(x) U(x, y; 0) L(y) U^\dagger(x, y, 1/T)] \rangle, \end{aligned} \quad (21)$$

$r = |\vec{x} - \vec{y}|.$

The correlators depend on the choice of the spatial transporters  $U(\vec{x}, \vec{y}; t)$ . Typically, a straight line connecting points  $\vec{x}$  and  $\vec{y}$  is used as a path in the gauge transporters, i.e. one deals with time-like rectangular cyclic Wilson loops. This object has been calculated at finite temperature in hard thermal loop (HTL) perturbation theory in context of perturbative calculations of the singlet potential introduced in the previous section and quarkonium spectral functions [8, 13, 14]. In the special gauge, where  $U(\vec{x}, \vec{y}; t) = 1$  the above correlators give the standard definition of the singlet and adjoint free energies of a static  $Q\bar{Q}$  pair

$$\exp(-F_1(r, T)/T) = \frac{1}{N} \langle \text{Tr} [L^\dagger(x) L(y)] \rangle, \quad (22)$$

$$\begin{aligned} \exp(-F_a(r, T)/T) &= \frac{1}{N^2 - 1} \langle \text{Tr} L^\dagger(x) \text{Tr} L(y) \rangle \\ &\quad - \frac{1}{N(N^2 - 1)} \langle \text{Tr} [L^\dagger(x) L(y)] \rangle. \end{aligned} \quad (23)$$

The singlet and adjoint free energies can be calculated at high temperature in leading order HTL approximation [7] resulting in

$$F_1(r, T) = -\frac{N^2 - 1}{2N} \frac{\alpha_s}{r} \exp(-m_D r) - \frac{(N^2 - 1)\alpha_s m_D}{2N}, \quad (24)$$

$$F_a(r, T) = \frac{1}{2N} \frac{\alpha_s}{r} \exp(-m_D r) - \frac{(N^2 - 1)\alpha_s m_D}{2N}, \quad (25)$$

with  $m_D = gT\sqrt{(N/3 + N_f/6)}$  being the leading order Debye mass and  $N_f$  is the number of quark flavors. At this order  $F_1$  and  $F_a$  are gauge independent or, in other words, do not depend on the choice of the parallel transporters  $U(\vec{x}, \vec{y}; t)$ . Note that at small distances ( $rm_D \ll 1$ ) the singlet free energy

$$F_1(r, T) \simeq -\frac{N^2 - 1}{2N} \frac{\alpha_s}{r} \quad (26)$$

is temperature independent and coincides with the zero temperature potential, while the adjoint free energy

$$F_a(r, T) \simeq \frac{1}{2N} \frac{\alpha_s}{r} - \frac{N}{2} \alpha_s m_D \quad (27)$$

depends on the temperature.

The physical free energy of a static quark anti-quark pair, i.e. the one related to the work that has to be done to separate the static charges by certain distance is given by the thermal average of the singlet and adjoint free energies [15]

$$\begin{aligned} \exp(-F(r, T)/T) &= \frac{1}{N^2} \exp(-F_1(r, T)/T) + \frac{N^2 - 1}{N^2} \exp(-F_a(r, T)/T) \\ &= \frac{1}{N^2} \langle \text{Tr} [L(x) \text{Tr} L(y)] \rangle \equiv \frac{1}{N^2} G(r, T). \end{aligned} \quad (28)$$

This quantity is explicitly gauge independent. In leading order HTL approximation the free energy is

$$F(r, T) = -\frac{(N^2 - 1)}{8N^2} \frac{\alpha_s^2}{r^2 T} \exp(-2m_D r). \quad (29)$$

The  $1/r^2$  behavior is due to partial cancellation between the singlet and adjoint contribution [15, 16] and has been confirmed by lattice calculations in the intermediate distance regime above the deconfinement transition [17, 18].

Using the transfer matrix one can show that in the confined phase

$$G_1(r, T) = \sum_{n=1}^{\infty} c_n(r) e^{-E_n(r, T)/T}, \quad (30)$$

$$G(r, T) = \sum_{n=1}^{\infty} e^{-E_n(r, T)/T}, \quad (31)$$

where  $E_n$  are the energy levels of static quark and anti-quark pair [19]. The coefficients  $c_n(r)$  depend on the choice of  $U(x, y; t)$  entering the static meson operator in Eqs. (18-19). Since the color averaged correlator  $G(r, T)$  corresponds to a gauge invariant measurable quantity it does not contain  $c_n$ . The lowest energy level is the usual static quark anti-quark potential, while the higher energy levels correspond to hybrid potentials [20–23]. Using multi-pole expansion in pNRQCD one can show that at short distances the hybrid potential corresponds to the adjoint potential up to non-perturbative constants [24]. Indeed, lattice calculations of the hybrid potentials indicate a repulsive short distance part [20–23]. Furthermore, the gap between



the static potential and the first hybrid potential can be estimated fairly well at short distances in perturbation theory [25].

If  $c_1 = 1$  the dominant contribution to  $G_a$  would be the first excited state  $E_2$ , i.e. the lowest hybrid potential which at short distances is related to the adjoint potential. In this sense  $G_a$  is related to static mesons with quark anti-quark in adjoint state. Numerical calculations show, however, that  $c_1$  is  $r$ -dependent and in general  $c_1(r) \neq 1$ . Thus  $G_a$  also receives contribution from  $E_1$  [19]. The lattice data suggests that  $c_1$  approaches unity at short distances [19] in accord with expectations based on perturbation theory, where  $c_1 = 1$  up to  $\mathcal{O}(\alpha_s^3)$  corrections [24]. Therefore at short distances,  $r \ll 1/T$  the color singlet and color averaged free energy are related  $F(r, T) = F_1(r, T) + T \ln(N^2 - 1)$ .

In the following we consider  $SU(2)$  and  $SU(3)$  gauge theories and refer to the adjoint state as triplet and octet, correspondingly.

#### 4.2. Lattice results on static meson correlators

Correlation function of static quarks have been extensively studied on the lattice since the pioneering work by McLerran and Svetitsky [15]. Most of these studies, however, considered only the color averaged correlator, i.e. the correlation function of two Polyakov loops (for the most complete analysis see Ref. [26] and references therein). Since both color singlet and color octet degrees of freedom contribute to the Polyakov loop correlator it has large temperature dependence even at short distances and it is not a very useful quantity if we want to learn something about quarkonium properties at high temperatures. As this has been pointed out in Refs. [27, 28] we need to know the quark anti-quark interactions in the singlet channel in order to learn about in-medium quarkonium properties. Therefore in recent years the singlet correlator has been computed on the lattice in  $SU(2)$  and  $SU(3)$  gauge theories [18, 29–32] as well as in full QCD with 3 and 2 flavors of dynamical quarks [33, 34]. Preliminary results also exist for 2+1 flavor QCD with physical value of the strange quark mass and light  $u, d$ -quark masses corresponding to pion mass of about  $220 \text{ MeV}$  [35, 36]. All these calculations use Coulomb gauge definition of the singlet correlator, i.e. the definition (22) with Coulomb gauge fixing.

The numerical results for  $SU(3)$  gauge theory are presented in Figure 1 and compared with the zero temperature potential. Here we used the string Ansatz for the zero temperature potential

$$V(r) = -\frac{\pi}{12r} + \sigma r, \quad (32)$$

since this form gives a very good description of the lattice data in  $SU(3)$  gauge theory [37]. To convert lattice units to physical units the value  $\sqrt{\sigma} = 420 \text{ MeV}$  has been used for the string tension. To remove the additive renormalization in the singlet free energy the lattice data have been normalized to  $V(r)$  given by Eq. (32) at the shortest distance available. As one can see from Figure 1 the singlet free energy is temperature independent at short distances and coincides with the zero

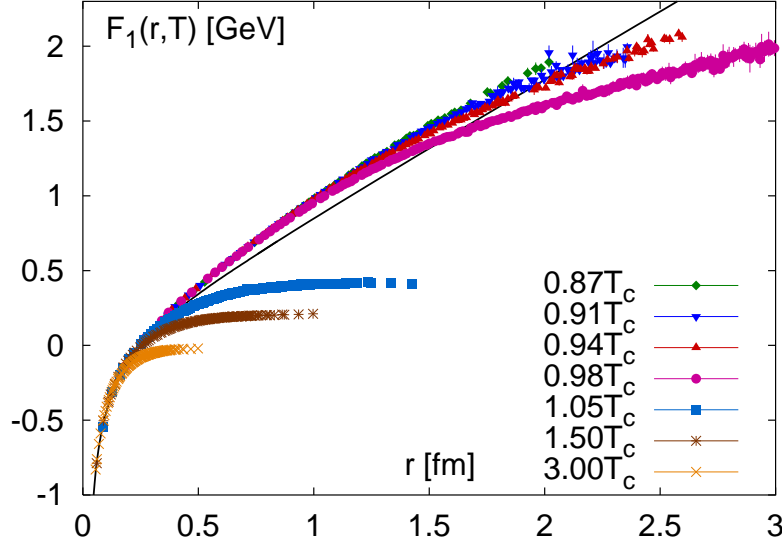


Fig. 1. The color singlet free energy singlet free energy in quenched QCD ( $SU(3)$  gauge theory) calculated in Coulomb gauge [29, 31, 32]. The solid line shows the zero temperature potential.

temperature potential. Below the deconfinement transition,  $T < T_c$ , it rises linearly, indicating confinement. The string tension at finite temperature is smaller than the zero temperature string tension  $\sigma$ . At large distances the singlet free energy is the same as the free energy determined from the Polyakov loop correlators and therefore the finite temperature string tension agrees with findings of Ref. [26]. Medium effects set in at distance  $r_{med} \simeq 0.4 \text{ fm}/(T/T_c)$  and we see exponential screening at distance  $r > 1/T$  [32]. In the intermediate distance regime  $0.5 \text{ fm} < r < 1.5 \text{ fm}$  we see that the singlet free energy is enhanced relative to the zero temperature potential. This is not a real physical effect but an artifact of the calculations. Similar effect has also been seen in  $SU(2)$  gauge theory [18, 19, 30]. At these distances the color singlet correlator is sensitive to the value of the coefficients  $c_n(r)$  in Eq. (30). Below we will show that the enhancement of the singlet free energy is due to the fact that  $c_1(r) < 1$  in this region.

Numerical results for the singlet free energy in 2+1 flavor QCD are shown in Figure 2. In this case a different normalization procedure has been used. The additive renormalization has been determined at zero temperature for each value of the lattice spacing used in the finite temperature calculations by matching the zero temperature potential to the string Ansatz (32) at distance  $r = r_0$ , with  $r_0$  being the Sommer scale [38]. This additive renormalization then has been used for the singlet free energy. For detailed discussion of the calculation of the static potential and its renormalization see Ref. [39]. As in quenched QCD the singlet

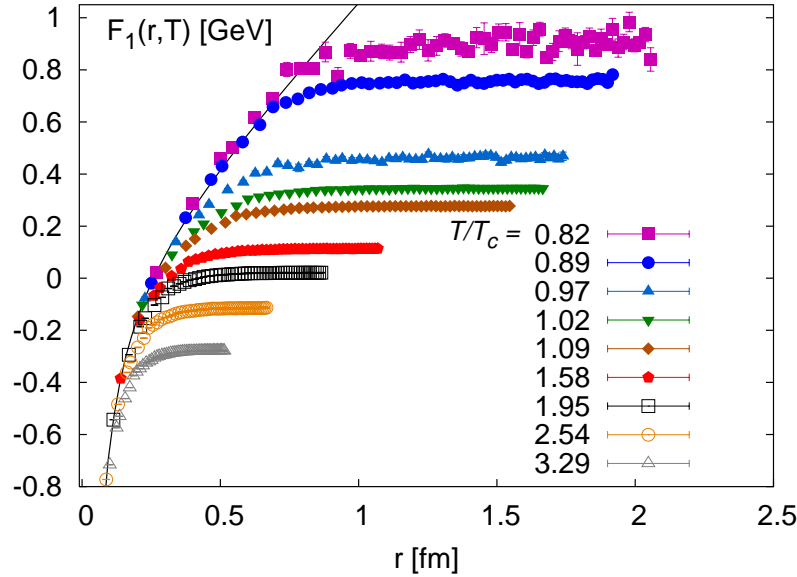


Fig. 2. The color singlet free energy in 2+1 flavor QCD [35, 36]. The solid line is the parametrization of the lattice data on the zero temperature potential from Ref. [39].

free energy is temperature independent at short distances and coincides with the zero temperature potential. At distances larger than the inverse temperature it is exponentially screened. The novel feature of the singlet free energy in full QCD is the string breaking, i.e. the fact that it approaches a constant at large separation. This happens because if the energy in the string exceeds the binding energy of a heavy-light meson the static quark and anti-quark are screened due to pair creation from the vacuum. This happens at distances of about 0.8 fm according to the figure. As temperature increases the distance where the singlet free energy flattens out becomes smaller and for sufficiently high temperatures turns out to be inversely proportional to the temperature. Thus string breaking smoothly turns into color screening as temperature increases.

#### 4.3. Color singlet correlator in $SU(2)$ gauge theory at low temperatures

For a better understanding of the temperature dependence of the singlet correlator and its physical interpretation the values of the overlap factors  $c_n(r)$  should be estimated. To extract the overlap factors we need to calculate the singlet correlators in the low temperature region, where only few energy levels contribute to the correlator. The calculations of the singlet correlator at low temperatures is difficult because of the rapidly decreasing signal to noise ratio. To overcome this difficulty it has been suggested to calculate Wilson loops with multilevel Luescher-Weisz algo-

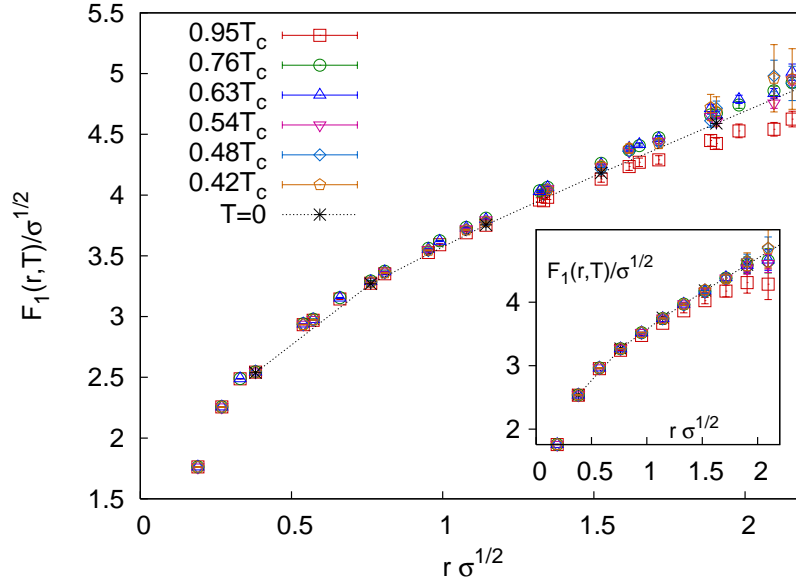


Fig. 3. The color singlet free energy in  $SU(2)$  gauge theory below the deconfinement temperature at  $\beta = 2.5$  calculated on  $32^3 \times N_\tau$  lattices. Also shown is the  $T = 0$  potential. The inset shows the color singlet free energy from which the contribution from the matrix element  $T \ln c_1$  has been subtracted.

rithm [40] instead of the Coulomb gauge fixing [41]. In this case the color singlet correlator defined by Eq. (20) is an expectation value of the gauge-invariant Wilson loop with gauge transporter  $U(\vec{x}, \vec{y}; t)$  being a product of the iteratively smeared spatial links.

Numerical calculations have been performed in  $SU(2)$  gauge theory using standard Wilson gauge action [41]. With the use of the multilevel algorithm it was possible to go down to temperatures as low as  $0.32T_c$  not accessible in the previous studies. It is well known that smearing increases the overlap with the ground state by removing the short distance fluctuations in the spatial links [42]. For this reason smearing also reduces the breaking of the rotational invariance to the level expected in the free theory. When no smearing is used the color singlet free energy,  $-T \ln G_1(r, T)$  shows a small but visible temperature dependence. The temperature dependence of the singlet free energy is significantly reduced when APE smearing is applied. The color singlet free energy for  $\beta = 2.5$  and 10 APE smearings is shown in Fig. 3. As one can see from the figure the color singlet free energy shows very mild temperature dependence in the confined phase with noticeable temperature effects appearing only at  $T = 0.95T_c$ .

Consider the expansion (30). The dominant contribution comes from the ground

state, so it is reasonable to fit the singlet correlator to the form

$$G_1(r, T) = c_1(r) \exp(-E_1(r)/T). \quad (33)$$

This allows to extract the matrix element  $c_1(r)$  using a simple exponential fit, which is shown in Fig. 4. When no APE smearing is used the value of  $c_1(r)$  strongly depends on the separation  $r$ . At small distances it shows a tendency of approaching unity as one would expect in perturbation theory. However,  $c_1(r)$  decreases with increasing distance  $r$ . At large distance its value is around  $0.3 - 0.5$ . Similar results for  $c_1(r)$  have been obtained in the study of  $SU(2)$  gauge theory in 3 dimensions [19]. When APE smearing is applied the  $r$ -dependence of the amplitude  $c_1(r)$  is largely reduced and its value is close to unity both for  $\beta = 2.5$  and  $\beta = 2.7$ . For  $\beta = 2.7$  we also see that increasing the number of smearing steps from 10 to 20 reduces the deviation of  $c_1(r)$  from unity.

As discussed in section 4.1 perturbation theory predicts that the deviation of  $c_1(r)$  from unity is of order  $\alpha_s^3$ . Therefore it can be made arbitrarily small by going to sufficiently small distances. It is known, however, that lattice perturbation theory converges very poorly. The main reason for this has been identified with the short distance fluctuations of the link variables, which makes their mean value very different from unity [43]. Smearing removes these short distance fluctuations and this is the reason why  $c_1(r)$  is much closer to unity when APE smearing is applied. Thus, almost the entire temperature dependence of the singlet free energy at distances  $0.5 < r\sqrt{\sigma} < 2$  is due to the deviation of  $c_1$  from unity and can be largely reduced by applying APE smearing to the links in the spatial gauge connections. To further demonstrate this point in the inset of Figure 3 we show the results for  $F_1(r, T) + T \ln c_1(r)$ . Clearly no temperature dependence can be seen in this quantity up to  $0.95T_c$ , where we see temperature dependence at distances  $r\sqrt{\sigma} \geq 1.5$  corresponding to the expected drop of the effective string tension.

#### 4.4. Color singlet free energy in the deconfined phase

The behavior of the color singlet free energy in the deconfined phase has been studied in Coulomb gauge [18, 29, 32–34] and from cyclic Wilson loops [41]. As discussed above at short distances it is temperature independent and coincides with the zero temperature potential. At large distances it approaches a constant  $F_\infty(T)$ , which monotonically decreases with the temperature. The constant  $F_\infty(T)$  is the free energy of two isolated static quarks, or equivalently of a quark anti-quark pair at infinite separation. Its value is therefore independent of the definition of the singlet correlator  $G_1(r, T)$  and is related to the renormalized Polyakov loop  $L_{ren}(T) = \exp(-F_\infty(T)/(2T))$  [29].

At leading order  $F_1(r, T) - F_\infty(T)$  is of Yukawa form (c.f. Eq. (24)). Therefore it is useful to define a quantity called the screening function

$$S(r, T) = r \cdot (F_1(r, T) - F_\infty(T)). \quad (34)$$

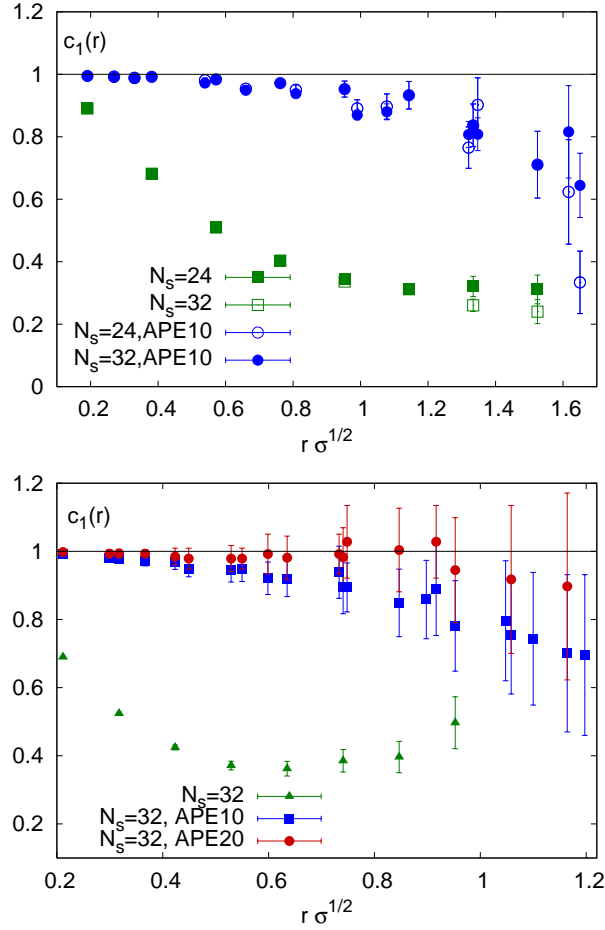


Fig. 4. The pre-exponential factor of the color singlet correlators as function of distance  $r$  for  $\beta = 2.5$  (top) and  $\beta = 2.7$  (bottom). Shown are results for unsmeared spatial links and 10 and 20 steps of APE smearing.

This quantity shows exponential decay at distances  $r > 1/T$  in the deconfined phase both in pure gauge theories [18, 32] and full QCD [34]. From its exponential decay the Debye screening mass has been determined and turns out to be about 40% larger than the leading order perturbative value.

It is interesting to study the screening function using the free energy determined from cyclic Wilson loops and make comparison with Coulomb gauge results. This analysis has been recently done in Ref. [41] for  $SU(2)$  gauge theory. The behavior of the screening function at different temperatures is shown in Fig. 5. At short distances ( $rT < 0.5$ ) the singlet free energy does not depend on the smearing level. Furthermore, it is very close to the free energy calculated in Coulomb gauge. At large

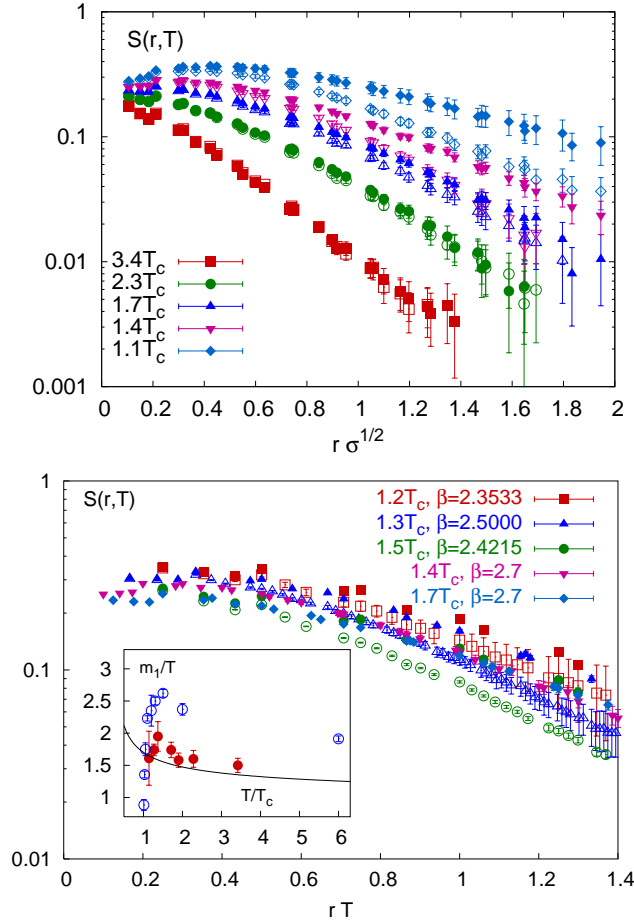


Fig. 5. The screening function  $S(r, T) = r(F_1(r, T) - F_\infty(T))$  in  $SU(2)$  gauge theory at different temperatures calculated for  $\beta = 2.7$  as function of  $r\sqrt{\sigma}$  (top) and as function of  $rT$  (bottom).

distances the screening function  $S(r, T)$  shows an exponential decay determined by a temperature dependent screening mass  $m_1(T)$ , which is equal to the leading order Debye mass up to the non-perturbative  $g^2$  corrections:  $m_1 = m_D + \mathcal{O}(g^2)$  [44, 45]. There is some dependence on the smearing level at larger distances which, however, disappears at high temperatures and with increasing the smearing level. In particular, for  $\beta \leq 2.5$  it turns out that there is no dependence on smearing level for 5 or more smearing steps. For  $\beta = 2.7$  10–20 steps are needed, depending on the temperature. Fitting the large distance behavior of the screening function by an exponential form  $\exp(-m_1(T)r)$  allows to determine the screening mass  $m_1(T)$ . In the inset of Fig. 5 the color singlet screening masses extracted from the fits are shown in comparison with the results obtained in Coulomb gauge in Ref. [18]. The

solid line is the leading order Debye mass calculated using 2-loop gauge coupling  $g(\mu = 2\pi T)$  in  $\overline{MS}$ -scheme. As we see from the figure the screening masses are smaller than those calculated in Coulomb gauge and agree well with the leading order perturbative prediction.

#### 4.5. Color adjoint free energy

The structure of Eqs. (20) and (21) shows that color adjoint correlator is given by a difference of the color averaged and singlet correlators. The color adjoint correlator in Coulomb gauge has been studied in pure gauge theory [7, 18], 3-flavor QCD [33] and 2-flavor QCD [34]. At low temperatures the color adjoint free energy turned out to be significantly smaller than the first hybrid potential contrary to the expectations. In fact at sufficiently large distance it was found to be identical to the singlet free energy. As has been pointed out in Ref. [19] this is due to the non-trivial  $r$ -dependence of the overlap factor  $c_1(r)$  and its deviation from unity.

We have shown in section 4.3 that deviations of the overlap factor  $c_1(r)$  from unity can be greatly reduced when one uses Wilson loops with the smeared spatial gauge connection. Therefore it is interesting to see how the adjoint free energy behaves in this approach. The numerical analysis has been done in  $SU(2)$  gauge theory [41] therefore below we will refer to the adjoint free energy as the triplet free energy. If we assume that only two states contribute to the Eqs. (30) and (31), then from Eq. (21) it follows that

$$F_3(r, T) = E_2(r) - T \ln \left( 1 - c_2(r) + \frac{1}{3}(1 - c_1(r))e^{\Delta E(r)/T} \right), \quad (35)$$

with  $\Delta E(r) = E_2(r) - E_1(r)$ . We have seen in section 4.3 that the temperature dependence of the singlet free energy is quite small. In any case it is considerably smaller than the temperature dependence of the averaged free energy. Therefore the contribution of the excited states to  $G_1(r, T)$  is quite small and it is reasonable to assume that  $c_2(r) \ll 1$ . From the analysis of the multipole expansion we also expect that at small distances,  $c_2(r) \sim (r\Lambda_{QCD})^4$  [46]. Thus, the temperature dependence of  $F_3(r, T)$  and its deviation from the hybrid state  $E_2(r)$  is due to small deviation of  $c_1(r)$  from unity. At low temperatures, when  $\Delta E \gg T$  these small deviations are amplified by the exponential factor. This can be easily verified by subtracting the correction  $T \ln(1 + \frac{1}{3}(1 - c_1)e^{\Delta E/T})$  from the triplet free energy and assuming that  $E_1(r)$  is given by the ground state potential and  $E_2(r)$  is given by the first hybrid potential as calculated in Ref. [23]. The numerical results are summarized in Fig. 6 which shows that after this correction is accounted for in the confined phase the triplet free energy at low temperatures agrees reasonably well with the first hybrid potential. As temperature increases more excited states contribute. In particular, at  $0.76T_c$  the value of the triplet free energy can be accounted for by including the next hybrid state [23]. However, at  $0.95T_c$  there are large temperature effects, which cannot be explained by including the contribution from only few excited states.



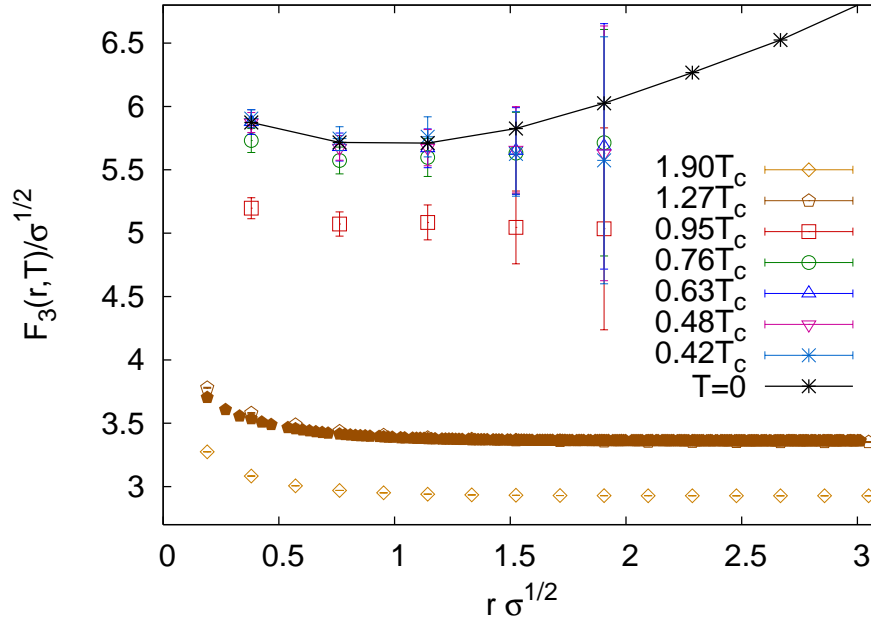


Fig. 6. The triplet free energy at different temperatures calculated at  $\beta = 2.5$ . The filled symbols correspond to calculations in Coulomb gauge. Also shown is the first hybrid potential calculated in [23].

In Fig. 6 we also show the triplet free energy above the deconfinement temperature compared to the calculations in Coulomb gauge [18]. It turns out to be much smaller than in the confined phase and agrees well with Coulomb gauge results. This means that the small deviation of the overlap factor  $c_1(r)$  from unity is unimportant in this case. The triplet free energy monotonically decreases with increasing temperature as expected in HTL perturbation theory (c.f. Eq. (25)). In the limit of high temperatures and short distances,  $r \ll 1/T$  we have  $E_2(r) = \alpha_s/(4r)$ ,  $\Delta E(r) = \alpha_s/r$ ,  $c_2(r) \simeq 0$  and  $c_1(r) = 1 + \mathcal{O}(\alpha_s^3)$ . Therefore we can expand the logarithm in Eq. (35) to get

$$F_3(r, T) = +\frac{1}{4} \frac{\alpha_s}{r} + \mathcal{O}(\alpha_s^3 T) + \mathcal{O}(\alpha_s m_D). \quad (36)$$

Thus the correction due to  $c_1(r) \neq 0$  is much smaller than the expected leading order thermal effects in the triplet free energy.

The strong temperature dependence of the adjoint free energy has been also observed in  $SU(3)$  gauge theory [7] and in full QCD [33, 34]. Although the adjoint free energy is strongly temperature dependent even at short distances its  $r$ -dependence is almost the same as  $r$ -dependence of the singlet free energy. The derivative of the adjoint free energy with respect to  $r$  is identical withing errors to that of the singlet free energy at short distances up to the Casimir factor, i.e.

$\Gamma$	$^{2S+1}L_J$	$J^{PC}$	$u\bar{u}$	$c\bar{c}(n=1)$	$c\bar{c}(n=2)$	$b\bar{b}(n=1)$	$b\bar{b}(n=2)$
$\gamma_5$	$^1S_0$	$0^{-+}$	$\pi$	$\eta_c$	$\eta'_c$	$\eta_b$	$\eta'_b$
$\gamma_s$	$^3S_1$	$1^{--}$	$\rho$	$J/\psi$	$\psi'$	$\Upsilon(1S)$	$\Upsilon(2S)$
$\gamma_s\gamma_{s'}$	$^1P_1$	$1^{+-}$	$b_1$	$h_c$		$h_b$	
1	$^3P_0$	$0^{++}$	$a_0$	$\chi_{c0}$		$\chi_{b0}(1P)$	$\chi_{b0}(2P)$
$\gamma_5\gamma_s$	$^3P_1$	$1^{++}$	$a_1$	$\chi_{c1}$		$\chi_{b1}(1P)$	$\chi_{b1}(2P)$
		$2^{++}$		$\chi_{c2}$		$\chi_{b2}(1P)$	$\chi_{b2}(2P)$

Table 1. Meson states in different channels

$$F'_a(r, T)/F'_1(r, T) = -1/(N^2 - 1) \text{ [7]}.$$

## 5. Quarkonium spectral functions

### 5.1. Meson correlators and spectral functions

Now we focus the discussion on the relation between the Euclidean meson correlators and spectral functions at finite temperature. The zero temperature limit is straightforward. Most dynamic properties of the finite temperature system are incorporated in the spectral function. The spectral function  $\sigma_H(p_0, \vec{p})$  for a given mesonic channel  $H$  in a system at temperature  $T$  can be defined through the Fourier transform of the real time two point functions  $D^>$  and  $D^<$  or equivalently as the imaginary part of the Fourier transformed retarded correlation function [47],

$$\begin{aligned} \sigma_H(p_0, \vec{p}) &= \frac{1}{2\pi} (D_H^>(p_0, \vec{p}) - D_H^<(p_0, \vec{p})) \\ &= \frac{1}{\pi} \text{Im} D_H^R(p_0, \vec{p}) \\ D_H^{>(<)}(p_0, \vec{p}) &= \int \frac{d^4p}{(2\pi)^4} e^{ip \cdot x} D_H^{>(<)}(x_0, \vec{x}) \end{aligned} \quad (37)$$

$$\begin{aligned} D_H^>(x_0, \vec{x}) &= \langle J_H(x_0, \vec{x}), J_H(0, \vec{0}) \rangle \\ D_H^<(x_0, \vec{x}) &= \langle J_H(0, \vec{0}), J_H(x_0, \vec{x}) \rangle, x_0 > 0 \end{aligned} \quad (38)$$

In essence  $\sigma_H$  is the Fourier transformation of the thermal average of the commutator  $[J(x), J(0)]$ .

In the present paper we study local meson operators of the form (c.f. (12) with  $\mathcal{U} = I$ )

$$J_H(t, x) = \bar{q}(t, x) \Gamma_H q(t, x) \quad (39)$$

with  $q$  a continuous real-time fermion position operator and

$$\Gamma_H = 1, \gamma_5, \gamma_\mu, \gamma_5\gamma_\mu, \gamma_\mu\gamma_\nu \quad (40)$$

for scalar, pseudo-scalar, vector, axial-vector and tensor channels. The relation of these quantum number channels to different meson states is given in Tab. 1.

The correlators  $D_H^{>(<)}(x_0, \vec{x})$  satisfy the well-known Kubo-Martin-Schwinger (KMS) condition [47]

$$D_H^{>}(x_0, \vec{x}) = D_H^{<}(x_0 + i/T, \vec{x}). \quad (41)$$

Inserting a complete set of states and using Eq. (41), one gets the expansion

$$\sigma_H(p_0, \vec{p}) = \frac{(2\pi)^2}{Z} \sum_{m,n} (e^{-E_n/T} \pm e^{-E_m/T}) \times \langle n | J_H(0) | m \rangle^2 \delta^4(p_\mu - k_\mu^n + k_\mu^m) \quad (42)$$

where  $Z$  is the partition function, and  $k^{n(m)}$  refers to the four-momenta of the state  $|n(m)\rangle$ .

A stable mesonic state contributes a  $\delta$  function-like peak to the spectral function:

$$\sigma_H(p_0, \vec{p}) = |\langle 0 | J_H | H \rangle|^2 \epsilon(p_0) \delta(p^2 - m_H^2), \quad (43)$$

where  $m_H$  is the mass of the state and  $\epsilon(p_0)$  is the sign function. For a quasi-particle in the medium one gets a smeared peak, with the width being the thermal width. As one increases the temperature the width increases and at sufficiently high temperatures, the contribution from the meson state in the spectral function may be sufficiently broad so that it is not very meaningful to speak of it as a well defined state any more. The spectral function as defined in Eq. (42) can be directly accessible by high energy heavy ion experiments. For example, the spectral function for the vector current is directly related to the differential thermal cross section for the production of dilepton pairs [48]:

$$\left. \frac{dW}{dp_0 d^3p} \right|_{\vec{p}=0} = \frac{5\alpha_{em}^2}{27\pi^2} \frac{1}{p_0^2 (e^{p_0/T} - 1)} \sigma_V(p_0, \vec{p}). \quad (44)$$

Then presence or absence of a bound state in the spectral function will manifest itself in the peak structure of the differential dilepton rate.

In finite temperature lattice calculations, one calculates Euclidean time propagators, usually projected to a given spatial momentum:

$$G_H(\tau, \vec{p}) = \int d^3x e^{i\vec{p}\cdot\vec{x}} \langle T_\tau J_H(\tau, \vec{x}) J_H(0, \vec{0}) \rangle \quad (45)$$

This quantity is an analytical continuation of  $D_H^{>}(x_0, \vec{p})$

$$G_H(\tau, \vec{p}) = D_H^{>}(-i\tau, \vec{p}). \quad (46)$$

Using this equation and the KMS condition one can easily show that  $G_H(\tau, \vec{p})$  is related to the spectral function, Eq. (37), by an integral equation (see e.g. appendix B of Ref. [49]):

$$G_H(\tau, \vec{p}) = \int_0^\infty d\omega \sigma(\omega, \vec{p})_H K(\omega, \tau) \quad (47)$$

$$K(\omega, \tau) = \frac{\cosh(\omega(\tau - 1/2T))}{\sinh(\omega/2T)}.$$

This equation is the basic equation for extracting the spectral function from meson correlators. Equation (47) is valid in the continuum. Formally the same spectral representation can be written for the Euclidean correlator calculated on the lattice  $G_H^{lat}(\tau, \vec{p})$ . The corresponding spectral function, however, will be distorted by the effect of the finite lattice spacing. These distortions have been calculated in the free theory [50, 51]. When discussing the numerical results in following sections the subscript  $H$  denoting different channels for meson correlators and spectral functions will be omitted.

### 5.2. Lattice formulations for charmonium physics

The quarkonium system at zero and finite temperature was studied in [52–55] using Wilson-type fermions

$$S_q^{Wilson} = \sum_x \bar{\psi}(x) \left[ m_0 + \not{D}^{Wilson} - \frac{c_{SW}}{2} \sum_{\mu, \nu} \sigma_{\mu\nu} F_{\mu\nu} \right] \psi(x), \quad (48)$$

where the Dirac operator is defined as

$$D_\mu^{Wilson} = \nabla_\mu - \frac{1}{2} \gamma_\mu \Delta_\mu \quad (49)$$

with

$$\begin{aligned} \nabla_\mu \psi(x) &= \frac{1}{2} \left[ U_\mu(x) \psi(x + \mu) - U_\mu^\dagger(x - \mu) \psi(x - \mu) \right] \\ \Delta_\mu \psi(x) &= \left[ U_\mu(x) \psi(x + \mu) + U_\mu^\dagger(x - \mu) \psi(x - \mu) - 2\psi(x) \right]. \end{aligned} \quad (50)$$

Furthermore,  $\sigma_{\mu, \nu} = \{\gamma_\mu, \gamma_\nu\}$  and the field strength tensor is defined as

$$\begin{aligned} F_{\mu\nu}(x) &= -\frac{i}{2} [Q_{\mu\nu} - Q_{\mu\nu}^\dagger] \\ 4Q_{\mu\nu}(x) &= U_\mu(x) U_\nu(x + \hat{\mu}) U_\mu^\dagger(x + \hat{\nu}) U_\nu^\dagger(x) + \\ &U_\nu(x) U_\mu^\dagger(x - \hat{\mu} + \hat{\nu}) U_\nu^\dagger(x - \hat{\mu}) U_\mu(x - \hat{\mu}) + \\ &U_\mu^\dagger(x - \hat{\mu}) U_\nu^\dagger(x - \hat{\mu} - \hat{\nu}) U_\mu(x - \hat{\mu} - \hat{\nu}) U_\nu(x - \hat{\nu}) + \\ &U_\nu^\dagger(x - \hat{\nu}) U_\mu(x - \hat{\nu}) U_\nu(x + \hat{\mu} - \hat{\nu}) U_\mu^\dagger(x). \end{aligned} \quad (51)$$

The last term in the brackets in Eq. (48) helps to suppress  $\mathcal{O}(a)$  lattice artifacts and is called the clover term. Formulations with  $c_{SW} \neq 0$  usually referred to as clover action. The standard Wilson action for fermions corresponds to  $c_{SW} = 0$ . In the lattice literature usually the form with the hopping parameter  $\kappa = 1/(2am_0 + 8)$  is used. In this form the fields need to be accordingly normalized  $\psi(x) \rightarrow \psi(x) a^{-3/2}/\sqrt{2\kappa}$ .

In [55] the anisotropic Fermilab formulation is used for the heavy quarks. The anisotropy allows to use fine temporal lattice spacings without significant increase in the computational cost. The study uses the quenched approximation and the

standard Wilson action in the gauge sector for which the relation between the bare  $\xi_0$  and the renormalized anisotropy  $\xi = a_s/a_t$  is known in a wide range of the gauge coupling  $\beta = 6/g^2$  [56].

The anisotropic clover action [57] is

$$S_q^\xi = \sum_x \bar{\psi}(x) \left[ m_0 + \nu_t \mathcal{D}_t^{\text{Wilson}} + \frac{\nu_s}{\xi_0} \sum_s \mathcal{D}_s^{\text{Wilson}} - \frac{1}{2} \left( C_{\text{sw}}^t \sum_s \sigma_{ts} F_{ts} + \frac{C_{\text{sw}}^s}{\xi_0} \sum_{s < s'} \sigma_{ss'} F_{ss'} \right) \right] \psi(x). \quad (53)$$

Because the lattice spacings in space and time directions are different the spatial and temporal Dirac operators as well as the clover terms have different coefficients. By tuning the clover coefficients according to the Fermilab prescription [57, 58] it is possible to reduce  $O(a_t m_0)$  discretization errors. We will refer to this formulation as anisotropic Fermilab formulation.

In the following we will show results from [55], where anisotropic Fermilab formulation was used as well as results from the study that used isotropic clover action with non-perturbatively determined values of  $c_{\text{SW}}$  [53]. In the study with anisotropic Fermilab action two values for the renormalized anisotropy  $\xi = 2, 4$  as well as  $\beta = 5.7, 5.9, 6.1, 6.5$  were used. These parameters correspond to temporal lattice spacings  $a_t^{-1} = 1.905 - 14.12$  GeV. To set the scale for the lattice spacing the traditional phenomenological value  $r_0 = 0.5$  fm for the Sommer scale [38] was used. The Sommer scale  $r_0$  has also been calculated for anisotropic Wilson action for  $\beta = 5.5 - 6.1$  [59]. Alternatively one can estimate the lattice spacing from the difference between the mass of  $^1P_1$  state and the spin averaged  $1S$  mass:  $\Delta M(^1P_1 - \overline{1S})$ . To a very good approximation this mass difference is not affected by fine and hyperfine splitting and thus is not very sensitive to quenching errors. It was found that close to the continuum limit the lattice spacing determined from  $\Delta M(^1P_1 - \overline{1S})$  is different from that determined from  $r_0$  by 10% [57, 60] if the phenomenological value  $r = 0.5$  fm is used. Using the value of  $r_0 = 0.469(7)$  determined in full QCD [61] would give a value for  $\Delta M(^1P_1 - \overline{1S})$  splitting which is closer to the experimental one, however, the  $\Delta M(\overline{2S} - \overline{1S})$  splitting would be even further away from the experimental value [60]. This problem is due to the quenched approximation.

In the studies with isotropic clover action the following values of the lattice gauge couplings have been used  $\beta = 6.499, 6.640$  and  $7.192$  [53, 62–64]. These correspond to lattice spacings  $a^{-1} = 4.04, 4.86$  and  $9.72$  GeV respectively if the value  $\sqrt{\sigma} = 420$  MeV for the string tension is used.

The continuum meson current in Eq. (39),  $J_H$  is related to the lattice current as

$$J_H = Z_H a_s^3 \bar{\psi} \Gamma_H \psi, \quad (54)$$

where  $\psi$  is the lattice quark field in Eq. (48). The renormalization constant  $Z_H$

can be calculated in perturbation theory or non-perturbatively. For isotropic clover action this has been done with both methods (see Ref. [53] and references therein).

### 5.3. Bayesian analysis of meson correlators

The obvious difficulty in the reconstruction of the spectral function from Eq. (47) is the fact that the Euclidean correlator is calculated only at  $\mathcal{O}(10)$  data points on the lattice, while for a reasonable discretization of the integral in Eq. (47) we need  $\mathcal{O}(100)$  degrees of freedom. The problem can be solved using Bayesian analysis of the correlator, where one looks for a spectral function which maximizes the conditional probability  $P[\sigma|DH]$  of having the spectral function  $\sigma$  given the data  $D$  and some prior knowledge  $H$  (for reviews see [65, 66]). Different Bayesian methods differ in the choice of the prior knowledge. One version of this analysis which is extensively used in the literature is the *Maximum Entropy Method* (MEM) [67, 68]. It has been used to study different correlation functions in Quantum Field Theory at zero and finite temperature [52–54, 62, 65, 68–79]. In this method the basic prior knowledge is the positivity of the spectral function and the prior knowledge is given by the Shannon - Janes entropy

$$S = \int d\omega \left[ \sigma(\omega) - m(\omega) - \sigma(\omega) \ln\left(\frac{\sigma(\omega)}{m(\omega)}\right) \right].$$

The real function  $m(\omega)$  is called the default model and parametrizes all additional prior knowledge about the spectral functions, e.g. such as the asymptotic behavior at high energy [65, 68]. For this case the conditional probability becomes

$$P[\sigma|DH] = \exp\left(-\frac{1}{2}\chi^2 + \alpha S\right), \quad (55)$$

with  $\chi^2$  being the standard likelihood function and  $\alpha$  a real parameter. Previously in the MEM analysis of the meson spectral functions the Bryan's algorithm was used [67]. A new algorithm was introduced in [55]. It is worth to make connection between this method and the Bryan algorithm. In both cases the true problem is number-of-data dimensional – in more dimensions the problem would be under-determined. To find the relevant subspace, the Bryan algorithm uses singular value decomposition, while the new algorithm finds the same relevant subspace by exact mathematical transformations. Although the method of identifying the subspace is different, the result is the same, and in both cases one proceeds with solving the original problem in this restricted subspace. The advantage of the new algorithm is that it is more stable numerically when one reconstructs quarkonium spectral functions at zero temperature.

The comparison of the two algorithms was done for the pseudo-scalar spectral function for  $\beta = 6.1$ ,  $\xi = 4$  [55]. The problem with the Bryan algorithm is that it does not work well for charmonium correlators if the time extent is sufficiently large, which is the case at low temperatures; the iterative procedure does not always converge. For instance at  $\beta = 6.1$ ,  $\xi = 4$  and  $16^3 \times 96$  lattice it was possible to get

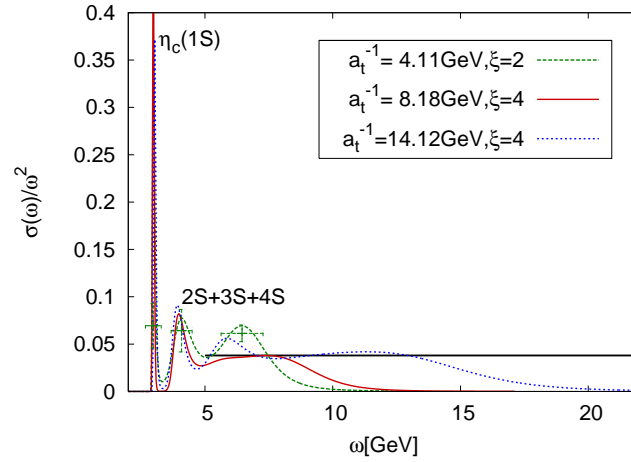


Fig. 7. The pseudo-scalar spectral function at zero temperature for three finest lattice spacings. The horizontal line corresponds to the spectral function in the free massless limit at zero lattice spacing.

the spectral functions using the Bryan algorithm only when using  $\tau_{max} = 24$  data points in the time direction. With the new algorithm there is no restriction on  $\tau_{max}$  which can be as large as  $N_\tau/2$ .

#### 5.4. Charmonium spectral functions at zero temperature

##### 5.4.1. Pseudo-scalar and vector spectral functions at zero temperature

In this subsection we discuss the results of Ref. [55] on charmonium spectral functions obtained using MEM. The zero temperature spectral functions for three different lattice spacings obtained by the new method from Ref. [55] are summarized in Fig. 7. Here the simple default model  $m(\omega) = 1$  (in units of the spatial lattice spacing) is used. To get a feeling for the statistical errors in the spectral functions its mean value in some interval  $I$  is calculated:

$$\bar{\sigma} = \frac{\int_I d\omega \sigma(\omega)}{\int_I d\omega}. \quad (56)$$

Then the error on  $\bar{\sigma}$  is calculated using standard jackknife method. These errors are shown in Fig. 7, where the length of the intervals are shown as horizontal error bars. As one can see from the figure, the  $\eta_c(1S)$  can be identified very well. The second peak is likely to correspond to excited states. Because of the heavy quark mass the splitting between different radial excitations is small and MEM cannot resolve different excitations individually but rather produces a second broad peak to which all radial excitation contribute. This can be seen from the fact that the amplitude of the second peak (i.e. the area under the peak) is more than two times larger than the first one. Physical considerations tell us that it should be smaller than the first

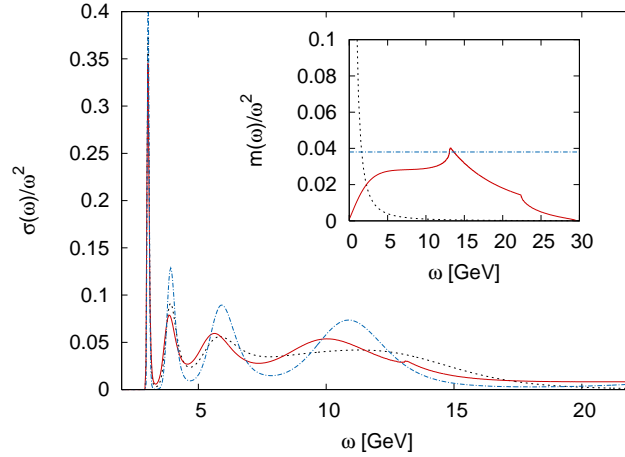


Fig. 8. The default model dependence of the pseudo-scalar spectral function at the finest lattice spacing ( $\beta = 6.5$ ). In the inset the default models corresponding to different spectral functions are shown.

amplitude if it was a  $2S$  state. When comparing amplitudes and peak positions from MEM analysis and from double exponential fits a very good agreement for the first peak and a fair agreement for the second peak are found. This gives confidence that at zero temperature charmonium properties can be reproduced well with MEM.

For energies larger than 5 GeV one probably sees a continuum in the spectral functions which is distorted by finite lattice spacing. In particular the spectral function is zero above some energy which scales roughly as  $a_s^{-1}$ . Note that for  $\omega < 5$  GeV the spectral function does not depend on the lattice spacing.

One should control how the result depends on the default model. In Fig. 8 we show the spectral function for three different default models. One can see that the default model dependence is significant only for  $\omega > 5$  GeV. This is not surprising as there are very few time slices which are sensitive to the spectral functions at  $\omega > 5$  GeV, while the first peak is well determined by the large distance behavior of the correlator.

The spectral function in the vector channel defined as

$$\sigma_V(\omega) = \frac{1}{3} \sum_i \sigma_{ii}(\omega), \quad (57)$$

was also calculated and is shown in Fig. 9 for the three finest lattice spacings. The conclusions which can be derived from this figure are similar to the ones discussed above for the pseudo-scalar channel. The first peak corresponds to the  $J/\psi(1S)$  state, the second peak most likely is a combination of  $2S$  and higher excited states, finally there is a continuum above 5 GeV which is, however, distorted by lattice artifacts. The similarity between the pseudo-scalar and vector channel is, of course, expected. The lower lying states in these channels differ only by small hyperfine



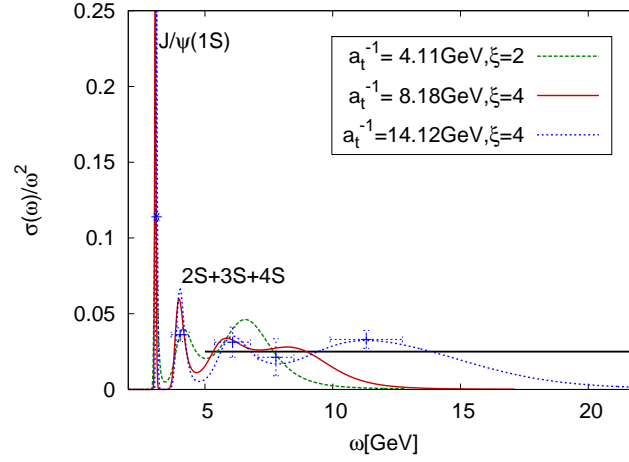


Fig. 9. The vector spectral function at zero temperature for three finest lattice spacings. The horizontal line is the spectral function in the free massless limit.

splitting.

#### 5.4.2. Spectral functions for $P$ states

The spectral functions in the scalar, axial-vector and tensor channels which have the  $1P$  charmonia as the ground state were also calculated in Ref. [55]. The scalar spectral functions reconstructed using MEM are shown in Fig. 10. The first peak corresponds to  $\chi_{c0}$  state, but it is not resolved as well as the ground state in the pseudo-scalar channel. This is due to the fact that the scalar correlator is considerably more noisy than the pseudo-scalar or vector correlator. This can be understood as follows. For the heavy quark mass the contribution of the ground state in the scalar channel is suppressed as  $1/m^2$  relative to the ground state contribution in the pseudo-scalar and vector channels, and therefore it is considerably smaller than the continuum contribution to the scalar correlator. For the two finest lattice spacings there is a second peak which may correspond to a combination of excited  $P$  states. Above  $\omega > 5$  GeV we see a continuum which is strongly distorted by lattice artifacts and probably also by MEM.

The spectral functions in the axial-vector and tensor channels are shown in Fig. 11. They look similar to the scalar spectral functions. As in the scalar channel the first peak is less pronounced than in the case of  $S$ -wave charmonium spectral functions, and it corresponds to  $\chi_{c1}$  and  $h_c$  state, respectively. The continuum part of the spectral function is again strongly distorted.

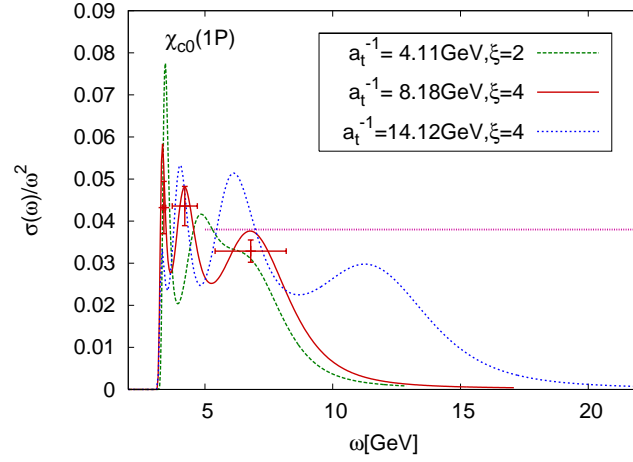


Fig. 10. The scalar spectral function at zero temperature for three finest lattice spacings.

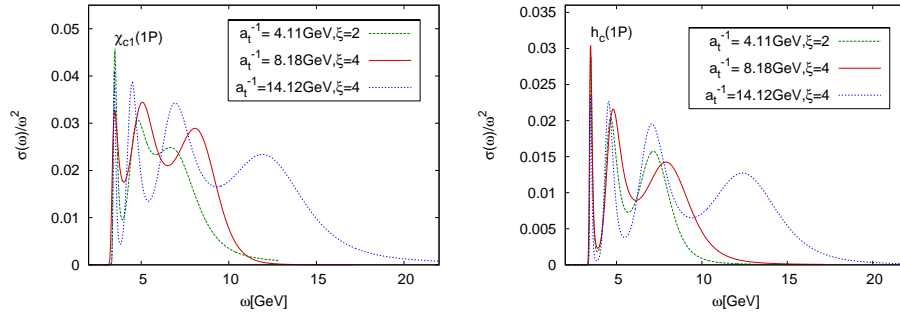


Fig. 11. The axial-vector (left) and tensor (right) spectral functions at zero temperature for three lattice spacings.

### 5.5. Charmonium correlators at finite temperature

The reconstruction of the spectral functions from lattice correlators is difficult already at zero temperatures. At finite temperature it is even more difficult to control the systematic errors in the spectral functions reconstructed from MEM. This is because with increasing temperature the maximal time extent  $\tau_{max}$  is decreasing as  $1/T$ . Also the number of data points available for the analysis becomes smaller. Therefore other methods which can give some information about the change of the spectral functions as the temperature is increasing are often used. The temperature dependence of the spectral function will manifest itself in the temperature dependence of the lattice correlator  $G(\tau, T)$ . Looking at Eq. (47) it is easy to see that the temperature dependence of  $G(\tau, T)$  comes from the temperature dependence of the spectral function  $\sigma(\omega, T)$  and the temperature dependence of the kernel  $K(\tau, \omega, T)$ .

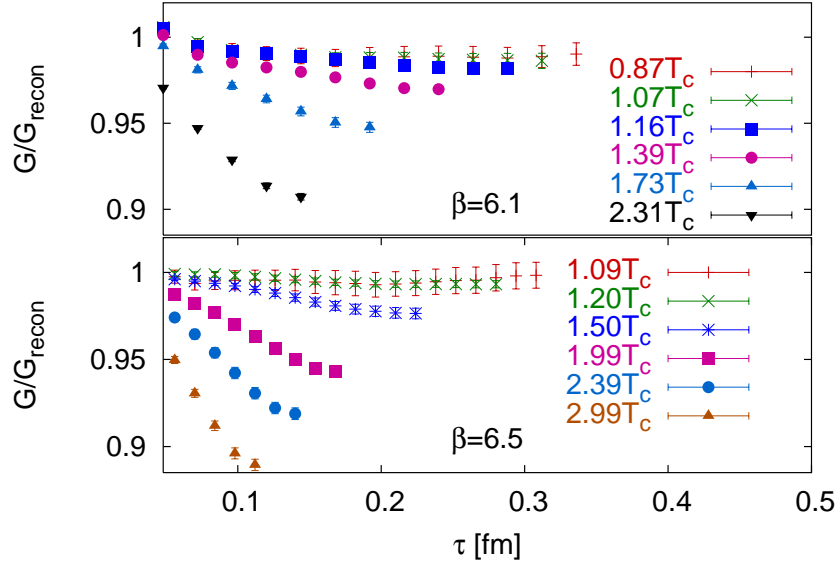


Fig. 12. The ratio  $G/G_{recon}$  for the pseudo-scalar channel for the two finer  $\xi = 4$  lattices.

To separate out the trivial temperature dependence due to  $K(\tau, \omega, T)$  one calculates the reconstructed correlator [53]

$$G_{recon}(\tau, T) = \int_0^\infty d\omega \sigma(\omega, T=0) K(\tau, \omega, T). \quad (58)$$

If the spectral function does not change with increasing temperature we expect  $G(\tau, T)/G_{recon}(\tau, T) = 1$ . In Ref. [55] an extensive study of the temperature dependence of this ratio for different channels at different lattice spacings was carried out.

#### 5.5.1. The pseudo-scalar correlators

First we present results from Ref. [55] for the temperature dependence of the pseudo-scalar correlators. In Fig. 12 we show numerical results for  $G/G_{recon}$  on lattices with  $\xi = 4$ . We see almost no change in the pseudo-scalar correlator till temperatures as high as  $1.2T_c$ . The temperature dependence of the pseudo-scalar correlator remains small for temperatures below  $1.5T_c$ . Medium modifications of the correlator slowly turn on as we increase the temperature above this value. From the figures it is clear that the temperature dependence of the correlators is not affected significantly by the finite lattice spacing. The very small temperature dependence of the pseudo-scalar correlator suggests that the corresponding ground state  $\eta_c(1S)$  may survive till temperatures as high as  $1.5T_c$ . The temperature dependence of the correlator found in this study is similar to that of Ref. [53], where isotropic lattices with

very small lattice spacings,  $a^{-1} = 4.86, 9.72$  GeV have been used. However, at temperatures higher than  $1.5T_c$  the deviations of  $G/G_{recon}$  from unity become slightly larger than those found in Ref. [53]. This is possibly due to the fact that cutoff effects are more important at higher temperatures. Thus despite similarities of the temperature dependence of the pseudo-scalar correlator to findings of Ref. [53] there are quantitative differences. One should note, however, statistical errors and systematic uncertainties are larger in the analysis presented in Ref. [53] than in Ref. [55]. In the study on isotropic lattices the ratio  $G/G_{recon}$  starts to depend more strongly on the temperature only around  $3T_c$  [53].

### 5.5.2. The $P$ -wave correlators

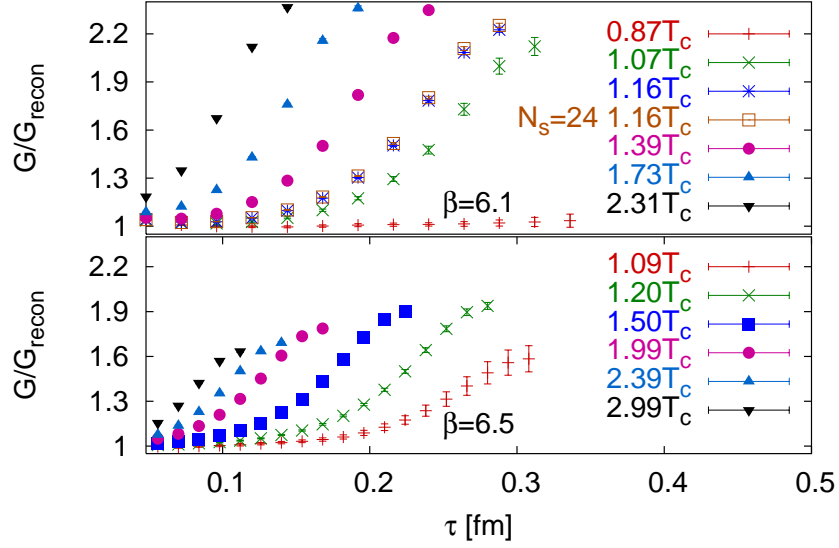
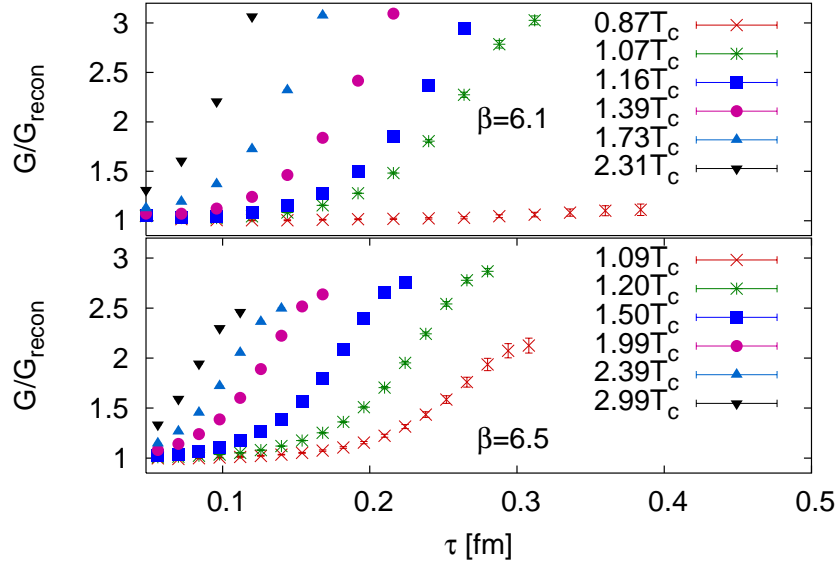
Next we present the temperature dependence of the scalar, axial-vector and tensor correlators corresponding to  $P$ -states. The  $\tau$  dependence of the scalar correlator was studied on  $\xi = 2, 4$  lattices [55]. The numerical results on fine lattices with  $\xi = 4$  are shown in Fig. 13. We see some differences in  $G/G_{recon}$  calculated at  $\beta = 6.1$  and  $\beta = 6.5$ . Thus the cutoff dependence of  $G/G_{recon}$  is larger in the scalar channel than in the pseudo-scalar one. For  $\beta = 6.1$  and  $\xi = 4$  the calculations were done on  $24^3 \times 24$  lattice to check finite volume effects. The corresponding results are shown in Fig. 13 indicating that the finite volume effects are small. On the finest lattice the enhancement of the scalar correlator is very similar to that found in calculations done on isotropic lattices [53], but small quantitative differences can be identified.

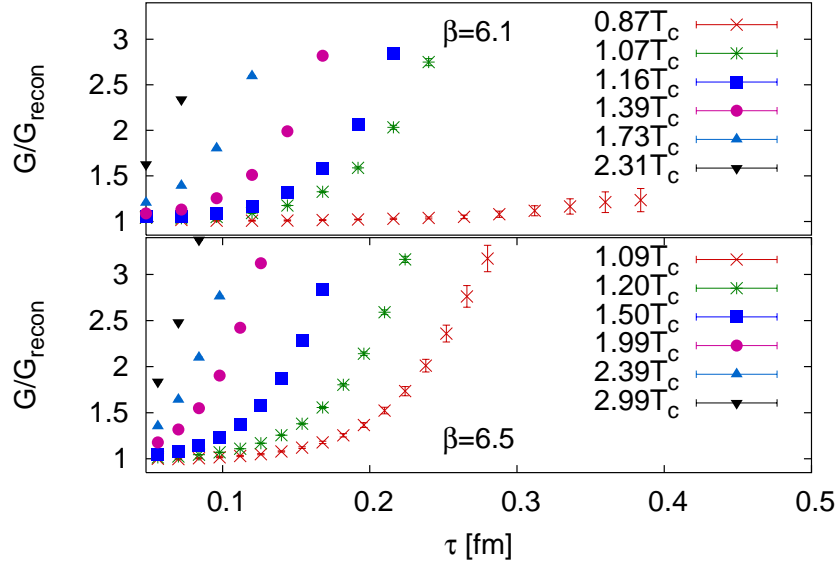
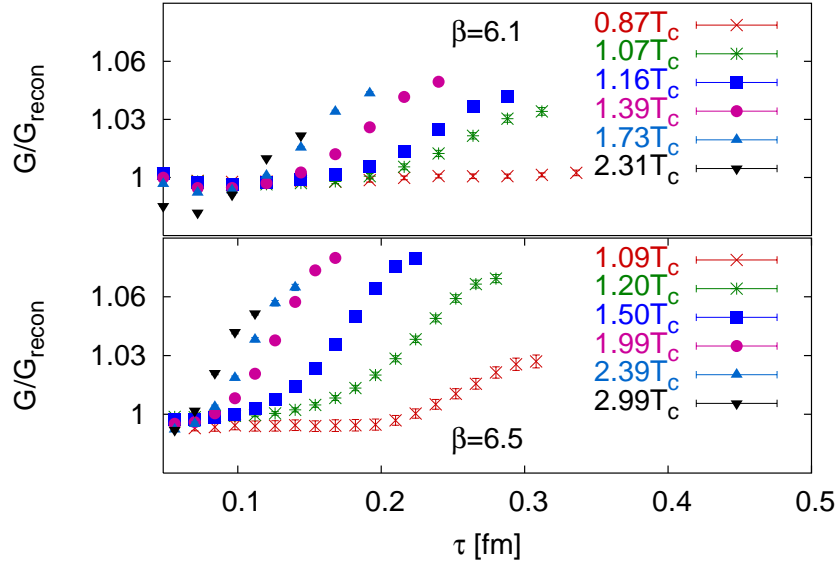
In Figs. 14 and 15 we show the temperature dependence of the axial-vector and tensor correlators respectively for  $\xi = 4$ . Qualitatively their behavior is very similar to the scalar correlator but the enhancement over the zero temperature result is larger. The results for the axial-vector correlators again are very similar to those published in Ref. [53]. The difference in  $G/G_{recon}$  calculated at  $\beta = 6.1$  and  $\beta = 6.5$  are smaller than in the scalar channel.

The large increase in the scalar, axial-vector and tensor correlators may be interpreted as indicator of strong modification of the corresponding spectral function and, possibly the dissolution of  $1P$  charmonia states. However, as we will see in the next sections the situation is more complicated. It has been noticed in [80] that the increase in  $G/G_{recon}$  may be due to the zero mode contribution.

### 5.5.3. The vector correlator

The numerical results for the vector correlator of Ref. [55] are shown in Fig. 16 for  $\xi = 4$ . As one can see from the figures the temperature dependence of  $G/G_{rec}$  is different from the pseudo-scalar case and this ratio is larger than unity for all lattice spacings. Similar results have been obtained on isotropic lattices [63]. The enhancement of the vector correlator is due to the presence of the transport contribution in the spectral function [49, 81] and will be discussed in section 5.10. Since

Fig. 13. The ratio  $G/G_{recon}$  for the scalar channel for the two finer  $\xi = 4$  lattices.Fig. 14. The ratio  $G/G_{recon}$  for the axial-vector channel for  $\xi = 4$  lattices.

Fig. 15. The ratio  $G/G_{recon}$  for the tensor channel for  $\xi = 4$  lattices.Fig. 16. The ratio  $G/G_{recon}$  for the vector channel for the two finer  $\xi = 4$  lattices.

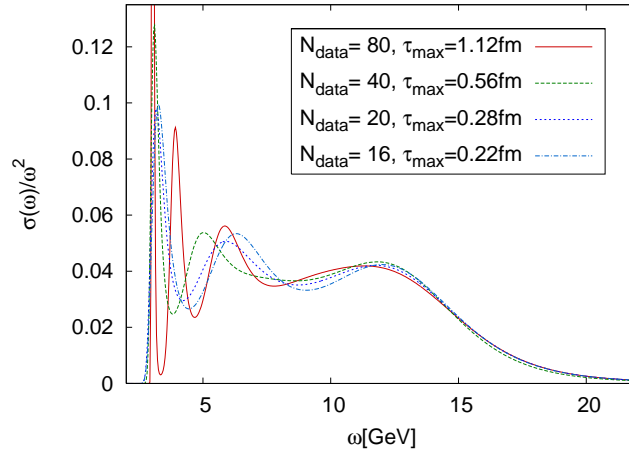


Fig. 17. The dependence of the reconstructed pseudo-scalar spectral function on the maximal temporal extent for  $\beta = 6.5$ . In the analysis the default model  $m(\omega) = 1$  has been used.

the vector current is conserved the vector correlator also carries information about the transport of heavy quarks in the plasma. This shows up as a peak in the spectral function at zero energy, leading to the observed enhancement in  $G/G_{recon}$ .

### 5.6. Charmonium spectral functions at finite temperature

In section 5.4 we have seen that using MEM one can reconstruct well the main features of the spectral function, in particular the ground state properties. At finite temperature the situation becomes worse because the temporal extent is decreasing. The maximal time separation is  $\tau_{max} = 1/(2T)$ . As a consequence it is no longer possible to isolate the ground state well. Also the number of available data points becomes smaller. While the later limitation can be overcome by using smaller and smaller lattice spacings in time direction the former limitation is always present. Therefore we should investigate systematic effects due to limited extent of the temporal direction. It appears that the pseudo-scalar channel is the most suitable case for this investigation as at zero temperature it is well under control and there is no contribution from heavy quark transport. To estimate the effect of limited temporal extent in Ref. [55] the spectral functions at zero temperature is calculated considering only the first  $N_{data}$  time-slices in the analysis for  $\beta = 6.5$ ,  $\xi = 4$ . The result of this calculation is shown in Fig. 17 where  $N_{data} = 80, 40, 20$  and  $16$ . The last two values correspond to the finite temperature lattices in the deconfined phase. In this case we see the first peak quite clearly. As one can see from the figure already for  $N_{data} = 40$  and  $\tau_{max} = 0.56$  fm the second peak corresponding to radial excitation is no longer visible and the first peak becomes significantly broader. The position of the first peak, however, is unchanged. As the number of data points is

further decreased ( $N_{data} = 20, 16$ ) we see further broadening of the first peak and a small shift of the peak position to higher energies. These systematic effects should be taken into account when analyzing the spectral functions at finite temperature. Therefore when studying the spectral functions at finite temperature we always compare with the zero temperature spectral functions reconstructed with the same number of data points and  $\tau_{max}$  as available at that temperature.

In Fig. 18 the spectral functions at different temperatures are shown together with the zero temperature spectral functions [55]. As a default model for  $T = 1.2T_c$  and  $T = 1.5T_c$   $m(\omega) = 0.01$  is used. For  $T = 2.0T_c$   $m(\omega) = 1$  is used since the use of  $m(\omega) = 0.01$  resulted in numerical problems in the MEM analysis. The figure shows that the pseudo-scalar spectral function is not modified till  $1.5T_c$  within the errors of the calculations. This is consistent with the conclusions of Ref. [53, 54]. One should note, however, that it is difficult to make any conclusive statement based on the shape of the spectral functions as this was done in the above mentioned works. The dependence of the reconstructed spectral functions on the default model  $m(\omega)$  is much stronger at finite temperature. The spectral functions were reconstructed using different types of default models. For all temperatures  $T \leq 1.5T_c$  the difference between the finite temperature spectral function and the zero temperature one is very small compared to the statistical errors for all default model considered here. In particular a use is made of the default models constructed from the high energy part of the lattice spectral functions calculated at zero temperature as this was done in Ref. [53]. The idea is that at sufficiently high energy the spectral function is dominated by the continuum and is temperature independent. Therefore it is suitable to provide the prior knowledge, i.e. the default model. With this default model the spectral functions were calculated at  $T = (1.07 - 1.5)T_c$  [55]. Very little temperature dependence of the spectral functions was found, see Fig. 19. Note, however, that for this choice of the default model no clear peak can be identified in the spectral functions if  $T \geq 1.2T_c$ .

The spectral function in the vector channel is also calculated [55]. The results are shown in Fig. 20 for the default model  $m(\omega) = 0.01$ . As this was already discussed in the previous section the basic difference between the pseudo-scalar and vector spectral functions at finite temperature is the presence of the transport peak at  $\omega \simeq 0$ . The difference of the temperature dependence of the vector and pseudo-scalar correlators is consistent with this assumption. The vector spectral function reconstructed with MEM shows no evidence of the transport peak at  $\omega \simeq 0$ . On the other hand the spectral function at  $1.2T_c$  differs from the zero temperature spectral function, in particular the first peak is shifted to smaller  $\omega$  values. We believe that this is a problem of the MEM analysis which cannot resolve the peak at  $\omega \simeq 0$  but instead mimics its effect by shifting the  $J/\psi$  peak to smaller  $\omega$ . Also at  $2.4T_c$  the spectral function extends to smaller  $\omega$  values than in the pseudo-scalar correlator which again indicates some structure at  $\omega \simeq 0$ . The analysis of the vector spectral functions using other choices for the default model always indicates that the spectral



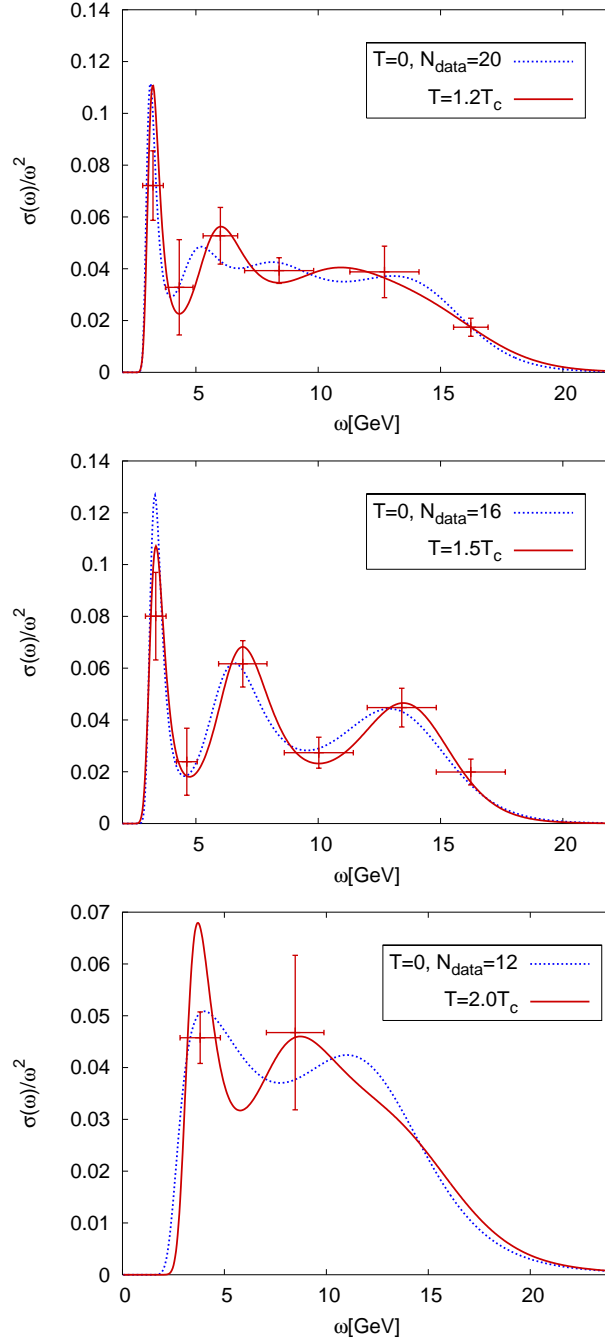


Fig. 18. The pseudo-scalar spectral function for  $\beta = 6.5$  and  $N_t = 40, 32, 20$  corresponding to temperatures  $1.2T_c$ ,  $1.5T_c$  and  $2.0T_c$ . In the analysis the default model  $m(\omega) = 0.01$  has been used for  $1.2T_c$  and  $1.5T_c$ , while for  $2.0T_c$  we used  $m(\omega) = 1$ .

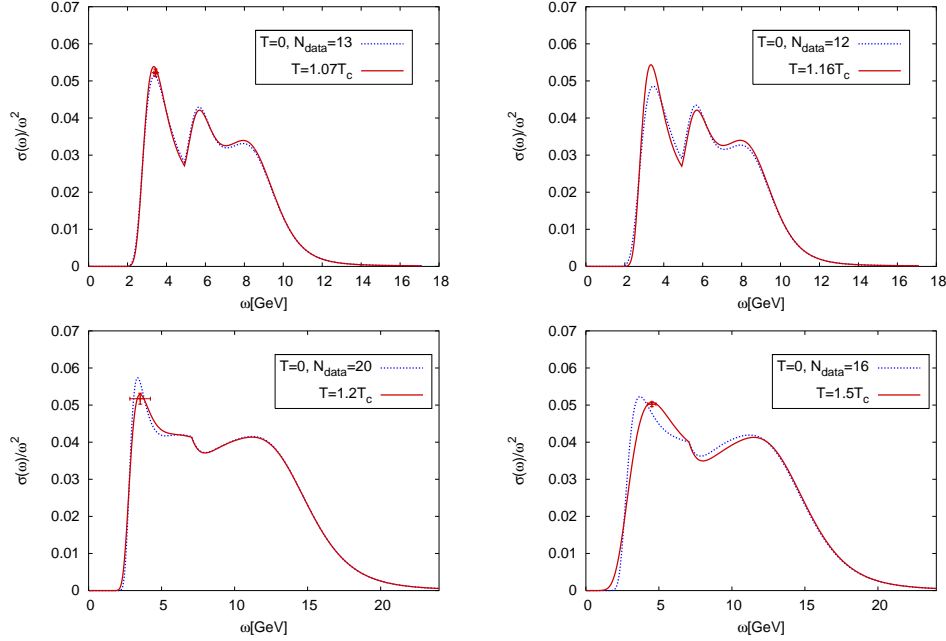


Fig. 19. The pseudo-scalar spectral function at different temperatures together with the zero temperature spectral functions reconstructed using default model coming from the high energy part of the zero temperature spectral function.

functions at finite temperature differs from the zero temperature spectral functions and extend to significantly smaller  $\omega$  values.

### 5.7. Charmonium correlators and spectral functions at finite momenta

So far we reviewed charmonia at zero spatial momentum, i.e. charmonia at rest in the heatbath's rest frame. It is certainly of interest to study the temperature dependence of correlators and spectral functions at non-zero spatial momentum. Such a study has been done using isotropic lattices with lattice spacing  $a^{-1} = 4.86\text{GeV}$  and  $9.72\text{ GeV}$  [63]. It has been found that the pseudo-scalar correlators are enhanced compared to the zero temperature correlators for non-vanishing spatial momenta, see Fig. 21. Furthermore, the enhancement of vector correlator at finite spatial momentum is larger than at zero spatial momentum.

In Ref. [55] the finite momentum pseudo-scalar correlators are calculated on anisotropic lattices at  $\beta = 6.1$ ,  $\xi = 4$  for different temperatures. The differences in  $G/G_{recon}$  calculated in this work and in Refs. [53, 63] are present already at zero momentum and are presumably due to finite lattice spacing errors. Apart from this the momentum dependence of the pseudo-scalar correlators is similar to the findings of Refs. [53, 63]. It would be interesting to see if the difference in

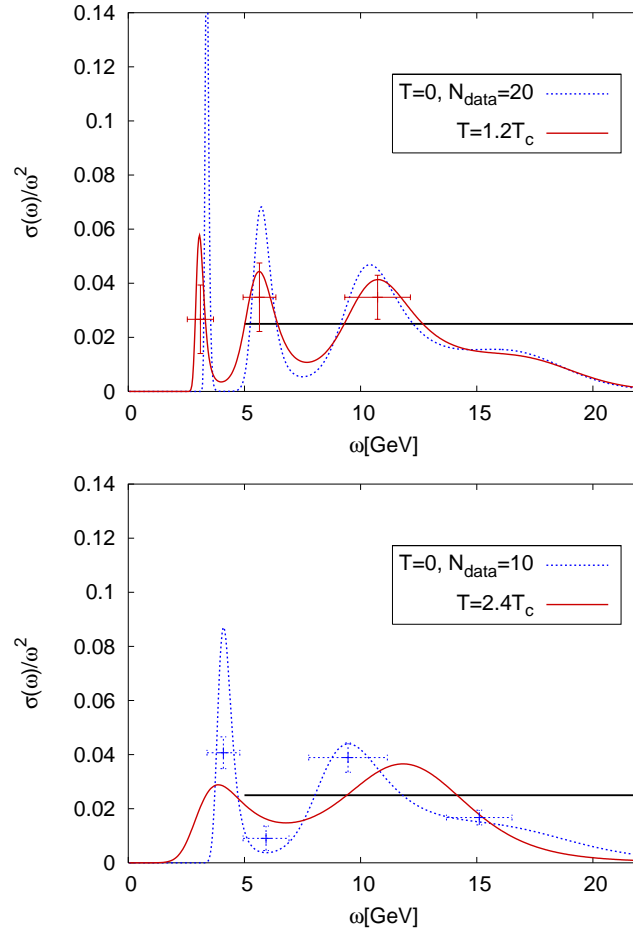


Fig. 20. The vector spectral function for  $\beta = 6.5$  and  $N_t = 40, 20$  corresponding to temperatures  $1.2T_c$  and  $2.4T_c$ . In the analysis the default model  $m(\omega) = 0.01$  has been used.

the temperature dependence of the correlators at zero and finite spatial momenta is due to a contribution to the spectral functions below the light cone at finite temperature [50, 51].

### 5.8. Bottomonium spectral functions at zero temperature

The use of Fermilab formulation described in the previous sections allows for a study of bottomonium for the same range of lattice spacings. Usually bottomonium is studied using lattice NRQCD (see e.g Ref. [82]). First study of bottomonium within the relativistic framework was presented in Ref. [83]. More recently it was studied in [55], where as before the lattice spacing is fixed by the Sommer scale  $r_0$ , assuming  $r_0 = 0.5\text{fm}$ . Note that the lattice spacings determined from  $r_0$  are about

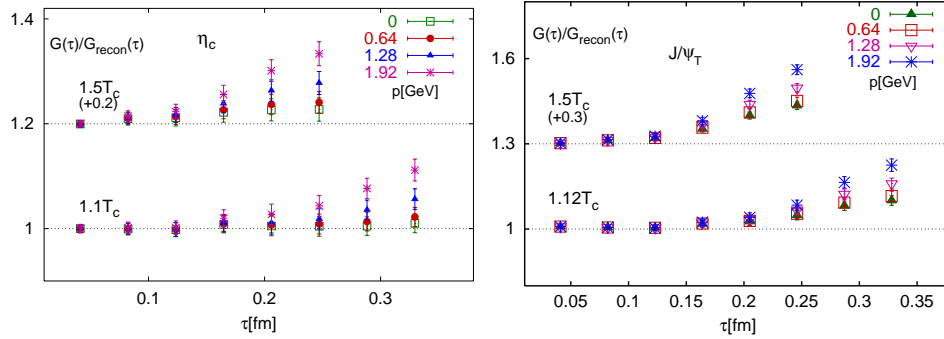


Fig. 21. Comparison of correlators at  $1.1 T_c$  and  $1.5 T_c$  for pseudoscalar and (transverse) vector charmonia with those reconstructed from spectral function at  $0.75 T_c$ .

20% smaller than in Ref. [83] where it was determined from bottomonium  $^1P_1 - \overline{1S}$  mass splitting. As the result the new estimates of the  $\Upsilon$  mass are smaller than those in Ref. [83]. However, one finds good agreement if the values of the lattice spacing quoted in Ref. [83] are used to calculate the physical masses.

Using MEM the spectral functions in different channels for three lattice spacings were analyzed. In Fig. 22 we show the spectral functions in the pseudo-scalar channel. Since the physical quark mass is different at different lattice spacings the horizontal scale was shifted by the difference of the calculated  $\Upsilon$ -mass and the corresponding experimental value. We can see that the first peak in the spectral function corresponds to the  $\eta_b(1S)$  state and its position is independent of the lattice spacing. The remaining details of the spectral functions are cut-off dependent and we cannot distinguish the excited states from the continuum. The position and the amplitude of the first peak in the spectral functions is in good agreement with the results of simple exponential fit. As in the charmonium case the maximal energy  $\omega_{max}$  for which the spectral function is non-zero scales approximately as  $a_s^{-1}$ . Similar results have been obtained in the vector channel.

The spectral function in the scalar channel is shown in Fig. 23. As it was the case for charmonium the correlators in this channel are more noisy than in the pseudo-scalar channel and as a result it is more difficult to reconstruct the spectral function. Nevertheless we are able to reconstruct the  $\chi_{b0}$  state which is the first peak in the spectral function. The peak position and the amplitude are in reasonable agreement with the result of the simple exponential fit.

### 5.9. Bottomonium at finite temperature

Besides calculating the bottomonium spectral function at zero temperature Ref. [55] presents a study of the temperature dependence of bottomonium correlators to see medium modification of bottomonia properties. In Fig. 24 we show  $G/G_{recon}$  for vector and pseudo-scalar channel at different lattice spacings. This ratio appears

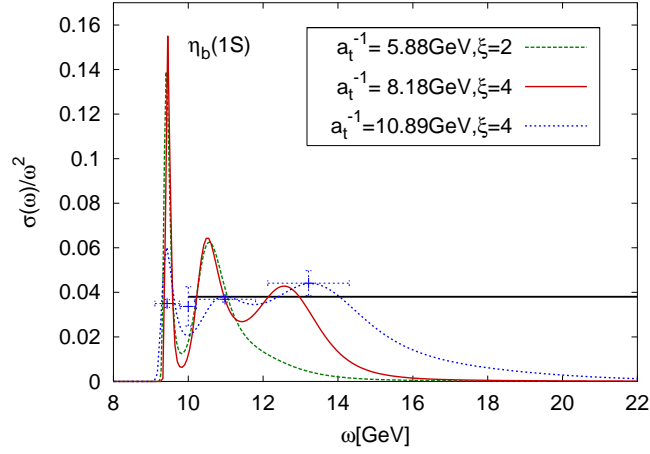


Fig. 22. The pseudo-scalar bottomonium spectral function at zero temperature for different lattice spacings.

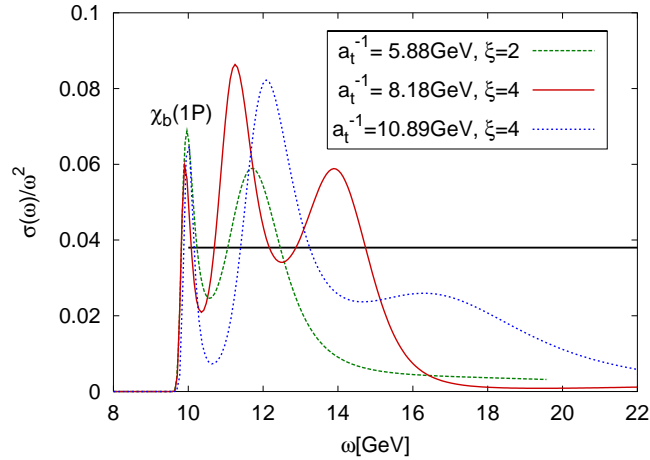


Fig. 23. The scalar bottomonium spectral function at zero temperature for different lattice spacings.

to be temperature independent and very close to unity up to quite high temperatures. This is consistent with the expectation that 1S bottomonia are smaller than 1S charmonia and thus are less effected by the medium. They could survive till significantly higher temperatures. Compared to charmonium case the difference between the pseudo-scalar and vector channels is smaller. This is also expected as the transport contribution which is responsible for this difference is proportional to  $\sim \exp(-m_{c,b}/T)$ , and thus is much smaller for bottom quarks (see the discussion in

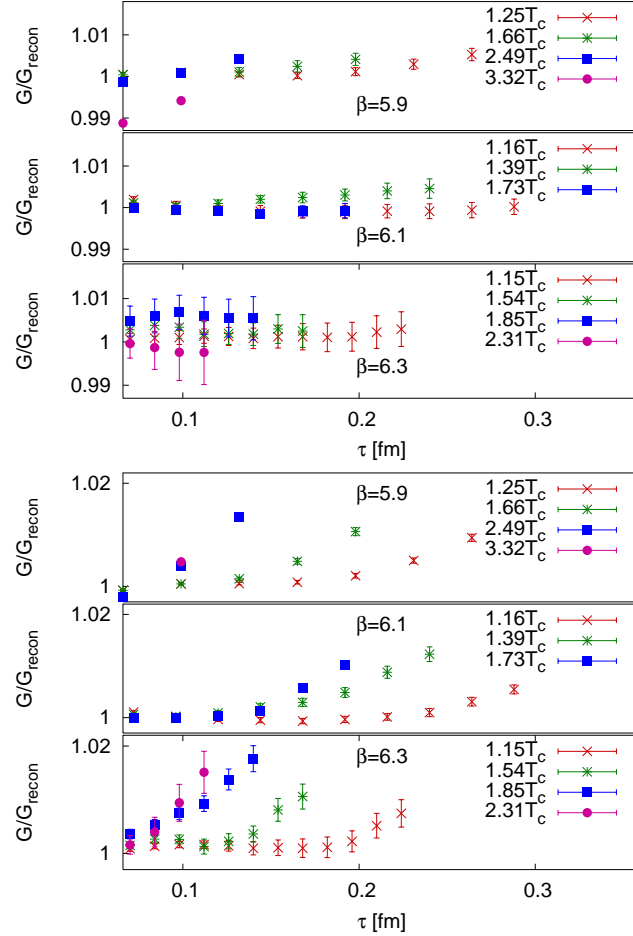


Fig. 24. The ratio  $G/G_{recon}$  in the pseudo-scalar (top) and vector channels at different lattice spacings.

the next section). Similar temperature dependence of the pseudo-scalar bottomonium correlator has been found in calculations with isotropic clover action [84].

The temperature dependence of the scalar correlator is shown in Fig. 25. Contrary to the pseudo-scalar and vector correlators it shows strong temperature dependence and  $G/G_{recon}$  is significantly larger than unity already at  $1.1T_c$ . Again, similar enhancement in  $G/G_{recon}$  has been observed in isotropic lattice calculations [84].

The spectral functions were reconstructed at finite temperature for  $\beta = 6.3$ . For the pseudo-scalar channel the results are shown in Fig. 26. As in the charmonium case we compare the finite temperature spectral function with the zero temperature spectral function obtained with the same number of data points and time interval.

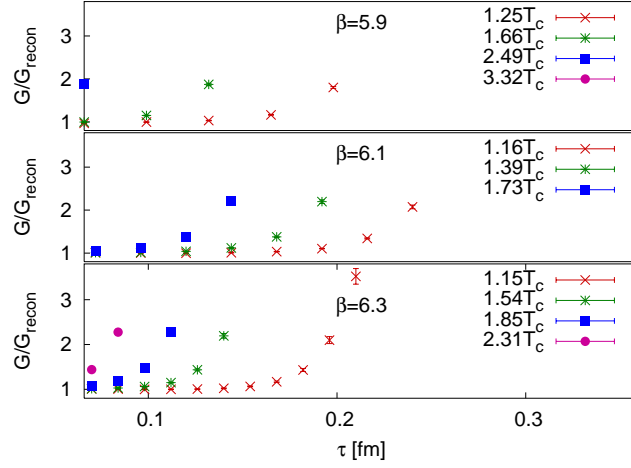


Fig. 25. The ratio  $G/G_{recon}$  in the scalar channel for different lattice spacings.

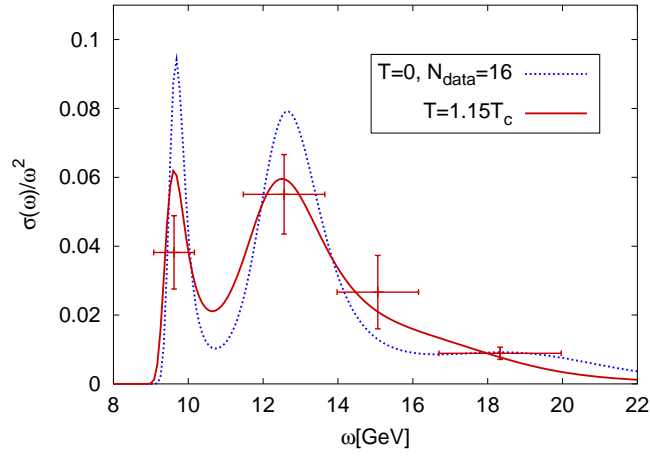


Fig. 26. The pseudo-scalar bottomonium spectral function at finite temperature.

As expected the spectral function shows no temperature dependence within errors. On the other hand it was not possible to reliably reconstruct the scalar spectral function at finite temperature due to numerical problems. Presumably much more statistics is needed to get some information about the scalar spectral function.

#### 5.10. Zero modes contribution

At finite temperature quarkonium spectral functions contain information about states containing a quark anti-quark pair as well as scattering of the external probe

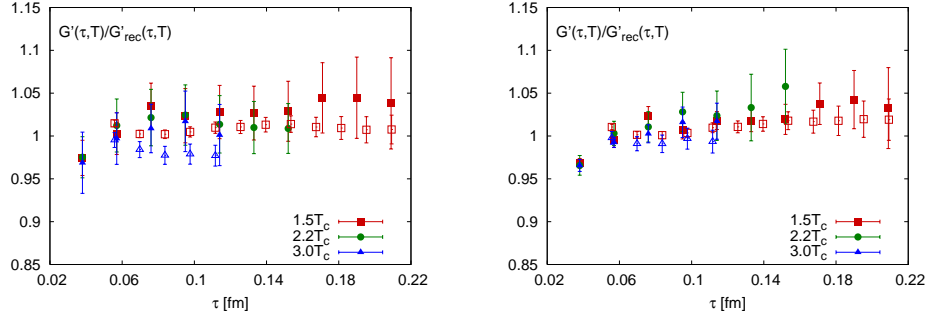


Fig. 27. The ratio of the derivatives  $G'(\tau, T)/G'_{rec}(\tau, T)$  in the scalar channel (left) and axial-vector channel (right) calculated at  $\beta = 7.192$ . The results from anisotropic lattice calculations at  $\beta = 6.5$  [55] are also shown (open symbols).

off a heavy quark from the medium. The later gives a contribution to the spectral function below the light cone ( $\omega < k$ ). In the limit of zero momentum it becomes  $\chi^i(T)\omega\delta(\omega)$  in the free theory. The generalized susceptibilities  $\chi^i(T)$  were calculated in Ref. [51] in the free theory. Interaction with the medium leads to the broadening of the delta function, which becomes a Lorentzian with a small width [81]. Because the quark anti-quark pair contributes to the spectral function at energies  $\omega > 2m$  it is reasonable to separate quarkonium spectral function into two terms [64]

$$\sigma^i(\omega, T) = \sigma_{\text{high}}^i(\omega, T) + \sigma_{\text{low}}^i(\omega, T). \quad (59)$$

Here  $\sigma_{\text{high}}^i(\omega, T)$  is the high energy part of the spectral functions which is non-zero only for  $\omega > 2m$  and describes the propagation of bound or unbound quark anti-quark pairs. On the other hand  $\sigma_{\text{low}}^i(\omega, T)$  receives the dominant contribution at  $\omega \simeq 0$ . Because the width of the peak at  $\omega \simeq 0$  is small the later gives an almost constant contribution to the Euclidean correlator, which is called the zero mode contribution. We can write an analogous decomposition for the Euclidean correlator

$$G^i(\tau, T) = G_{\text{high}}^i(\tau, T) + G_{\text{low}}^i(\tau, T). \quad (60)$$

To a very good approximation  $G_{\text{low}}^i(\tau, T) = \chi^i(T)T$ , i.e. constant.

In the previous sections we used the ratio  $G(\tau, T)/G_{rec}(\tau, T)$  to study the temperature dependence of the correlators. This dependence comes separately from the high energy part and low energy part, which gives the zero mode contribution. The zero mode contribution is absent in the derivative of the correlator with respect to  $\tau$ . Therefore one can study the temperature dependence of the correlators induced by change of bound state properties and/or its dissolution by considering the ratio of the derivatives of the correlators  $G'(\tau, T)/G'_{rec}(\tau, T)$ .

The temperature dependence of scalar (13) and axial-vector correlators (14) has been presented in previous sections in terms of  $G/G_{rec}$ . It is temperature independent in the confined phase and shows large enhancement in the deconfined



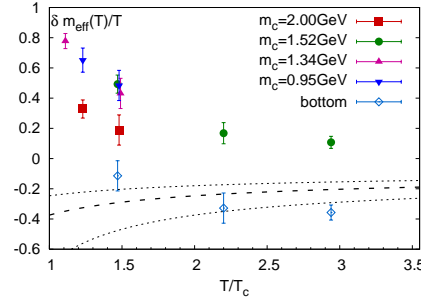


Fig. 28. The thermal mass correction as function of the temperature. The dashed line and the band correspond to the perturbative prediction of the thermal mass correction.

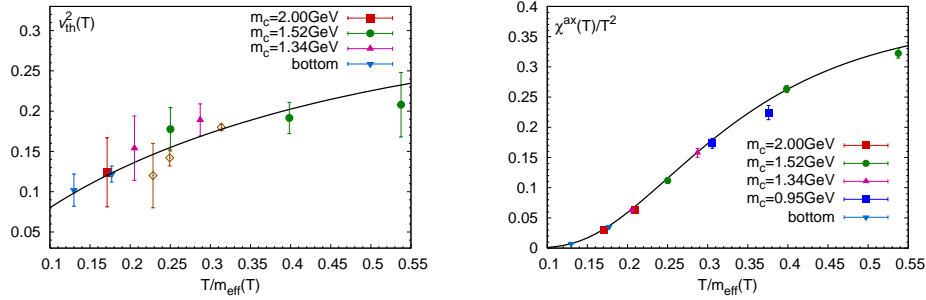


Fig. 29. The thermal velocity of heavy quarks (left) and the zero mode contribution to the axial-vector correlator  $G_{\text{low}}^{ax}/T^3 = \chi^{ax}/T^2$  (right). The lines show the prediction of the quasi-particle model with  $m_{\text{eff}}(T)$ . The open symbols show the thermal velocity squared estimated on anisotropic lattices [55].

phase. This large enhancement is present both in charmonium and bottomonium correlators. To eliminate the zero mode contribution the derivative of the correlators and the corresponding ratio  $G'(\tau, T)/G'_{\text{recon}}(\tau, T)$  have been calculated in [64] using isotropic lattices. The numerical results for this ratio at  $\beta = 7.192$  are shown in Fig. 27. The results from anisotropic lattices [55] are also shown. There is good agreement between the results obtained from isotropic and anisotropic lattices. As one can see from Fig. 27  $G'(\tau, T)/G'_{\text{recon}}(\tau, T)$  shows very little temperature dependence and is close to unity. This means that almost the entire temperature dependence of the scalar and axial-vector correlators is due to zero mode contribution and  $G_{\text{high}}(\tau, T)$  is temperature independent. The temperature dependence of the S-states seen in previous sections is also greatly reduced and the agreement between isotropic and anisotropic calculations is better for the ratio of derivatives. For the pseudo-scalar channel this behavior can be explained by the presence of a small negative zero mode [64].

Since the high energy part of the quarkonium correlators turns out to be temperature independent to very good approximation one can assume that  $G_{\text{high}}^i(\tau, T) \simeq G_{\text{recon}}^i(\tau, T)$ . Then the low energy part of the correlators, i.e. the zero mode contribution can be evaluated as  $G_{\text{low}}^i(\tau, T) = G^i(\tau, T) - G_{\text{recon}}^i(\tau, T)$  [64]. Current lattice data are not precise enough to see a clear  $\tau$  dependence in  $G_{\text{low}}^i(\tau, T)$  and it is compatible with being a constant. Therefore, one could take the value of low energy part of the correlator at the midpoint as an estimate for the zero mode contribution,  $G_{\text{low}}^i(\tau = 1/(2T), T) = T\chi^i(T)$ .

The zero mode contribution is related to the propagation of single (unbound) heavy quark in the medium. Therefore, it is natural to describe its temperature dependence in terms of a quasi-particle model with effective temperature dependent heavy quark masses. Since the temporal component of the vector correlator has no high energy part, i.e.  $G^{vc0}(\tau, T) = -T\chi^{vc0}(T) = -T\chi(T)$  it is most suitable for fixing the effective quark mass. Matching the lattice data to the free theory expression for  $\chi(T)$  one can determine the effective quasiparticle masses  $m_{\text{eff}}$  [64]. The results of this analysis are shown in Fig. 28 for different values of the constituent heavy quark mass, including the bottom quarks, in terms of thermal mass correction  $\delta m_{\text{eff}}(T) = m_{\text{eff}}(T) - m$ . As one can see from the figure the thermal mass correction decreases monotonically with increasing the constituent quark mass and increasing temperature for bottom quarks it is not incompatible with the leading-order perturbative prediction

$$\delta m_{\text{eff}} = -\frac{4}{3} \frac{g^2(T)}{4\pi} m_D, \quad (61)$$

with  $m_D = g(T)T$  being the perturbative Debye mass ( $N_f = 0$  because we work in the quenched approximation).

Having determined the effective heavy quark mass we can study the zero mode contribution in other channels. If the quasi-particle model is correct the zero mode contribution should be a function of  $m_{\text{eff}}/T$  only. Therefore in Fig. 29 the temperature dependence of zero mode contribution for the vector and axial-vector channel is shown as function of  $T/m_{\text{eff}}$ . Indeed, all the lattice data seem to fall on one curve within errors, which agrees with the quasi-particle model prediction shown as the black lines. For the vector channel we show the data in terms of the ratio  $G_{\text{low}}^{vc}(T)/G^{vc0}$ , where  $G_{\text{low}}^{vc}(T)$  is the sum over all spatial components. This is because this quantity does not depend on the renormalization [64] and has simple physical interpretation in terms of averaged thermal velocity squared  $v_{\text{th}}^2$ . The later follows from the fact that due to the large quark mass the Boltzmann approximation can be used and we have

$$\frac{G_{\text{low}}^{vc}(T)}{G^{vc0}(T)} \simeq \left( \int d^3p \frac{p^2}{E_p^2} e^{-E_p/T} \right) / \left( \int d^3p e^{-E_p/T} \right) = v_{\text{th}}^2. \quad (62)$$

The zero mode contribution in the vector channel has also been studied on anisotropic lattices [55] and in Fig. 29 we also show the corresponding results for thermal velocity squared.

## 6. Potential models at finite temperature

Quarkonium properties at finite temperature have been studied in potential models since the famous paper of Matsui and Satz [1] (for recent review see [2]). The basic idea behind this is that color screening will modify the potential, which becomes short range and cannot support bound states of heavy quarks at sufficiently high temperatures. As discussed in section 2 this approach can be justified if there is a separation of the scales related to binding energy and other scales in the problem, like the inverse size of the bound states and the temperature. Close to the QCD transition this separation of scales is not obvious, however, the lattice calculation of static quark correlators, discussed in section 4 show that screening effects are very strong already in the transition region. In fact, correlation functions of static quark anti-quark pair show significant temperature modifications already at distances similar to quarkonium size. Therefore, we may expect the most of quarkonium bound states dissolve in the deconfined phase at temperatures close to the transition temperature. This seemingly contradicts to the small temperature dependence of quarkonium correlators and spectral functions discussed in the previous section.

Due to the heavy quark mass quarkonium spectral functions can be calculated in the potential approach by relating the spectral functions in the threshold region to the non-relativistic Green function [14, 85, 86]

$$\sigma(\omega) = K \frac{6}{\pi} \text{Im} G^{nr}(\vec{r}, \vec{r}', E)|_{\vec{r}=\vec{r}'=0}, \quad (63)$$

$$\sigma(\omega) = K \frac{6}{\pi} \frac{1}{m_c^2} \text{Im} \vec{\nabla} \cdot \vec{\nabla}' G^{nr}(\vec{r}, \vec{r}', E)|_{\vec{r}=\vec{r}'=0}, \quad (64)$$

for  $S$ -wave, and  $P$ -wave quarkonia, respectively. Here  $E = \omega - 2m$ . The pre-factor  $K$  accounts for relativistic and radiative corrections. The non-relativistic Green function is calculated from the Schrödinger equation with a delta-function on the right hand side. Away from the threshold the spectral function is matched to the perturbative result. It has been shown that this approach can provide a fair description of quarkonium correlators at zero temperature [87]. Other approaches to calculate quarkonium spectral functions in potential models were proposed in Refs. [49, 88–91]. Close to the transition temperature the perturbative calculations of the potential are not applicable. Therefore in Ref. [85] the singlet free energy calculated in quenched lattice QCD has been used to construct the potential. The drawback of this approach is that there is no one to one correspondence between the singlet free energy and the potential in the non-perturbative domain. Therefore in Ref. [85] several possible forms of the potential compatible with the lattice data have been considered. Furthermore, lattice calculations do not have much information about the imaginary part of the potential. Therefore the imaginary part of the potential has been approximated by a small constant term. The results of the calculations of the charmonium and bottomonium spectral functions for  $S$ -wave are shown in Fig.30. In the case of charmonium all bound states are melted at temperatures higher than  $1.2T_c$ . We see, however a significant threshold enhancement,

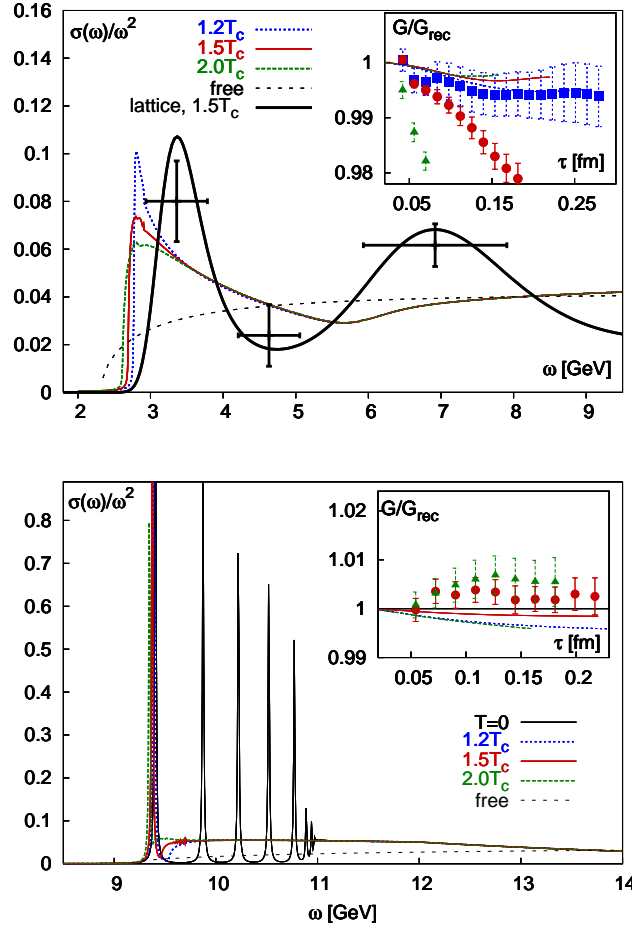


Fig. 30. The charmonium (top) and bottomonium (bottom) spectral functions at different temperatures. For charmonium we also show the spectral functions from lattice QCD obtained from the MEM at  $1.5T_c$ . The error-bars on the lattice spectral function correspond to the statistical error of the spectral function integrated in the  $\omega$ -interval corresponding to the horizontal error-bars. The insets show the corresponding ratio  $G/G_{recon}$  together with the results from anisotropic lattice calculations [55]. For charmonium, lattice calculations of  $G/G_{recon}$  are shown for  $T = 1.2T_c$  (squares),  $1.5T_c$  (circles), and  $2.0T_c$  (triangles). For bottomonium lattice data are shown for  $T = 1.5T_c$  (circles) and  $1.8T_c$  (triangles).

i.e. near the threshold the spectral function is much larger than in the free case. In the bottomonium case only the ground state survives in the deconfined phase. At temperatures above  $2T_c$  we see the melting of the ground state as well.

Quarkonium spectral functions calculated using the perturbative potential, where the imaginary part is fully taken into account, show similar qualitative features [14, 86]. Here too a significant threshold enhancement is seen. The imaginary part of the potential plays an important role in weakening the bound state peak

or transforming it to mere threshold enhancement. Let us note that the next-to-leading order perturbative correction to the quarkonium spectral functions also give rise to significant enhancement in the threshold region [92].

From the spectral functions we can calculate the quarkonium correlation functions in Euclidean time  $G(\tau, T)$  and compare them to the available lattice data. This comparison is shown in Fig. 30 for the ratio  $G(\tau, T)/G_{recon}(\tau, T)$ . As one can see from the figure the melting of bound states does not lead to large change in the Euclidean correlation functions. The ratio  $G(\tau, T)/G_{recon}(\tau, T)$  calculated in the potential model is flat and temperature independent in agreement with lattice calculations. This means that threshold enhancement can compensate for melting of bound states in terms of the Euclidean correlators. Spectral functions of  $P$ -wave quarkonium have been also calculated [14, 85] and show significant threshold enhancement as well. As the consequence the ratio of the derivatives  $G'(\tau, T)/G'_{recon}(\tau, T)$  is temperature independent and close to unity [85] in agreement with lattice calculations shown in the previous section.

The analysis discussed above has been done in quenched QCD. This is because only in quenched QCD we have sufficiently precise lattice calculations of quarkonium correlators. Potential model calculations of the spectral functions have been extended to 2+1 flavor QCD using the lattice data discussed in section 4. These calculations show that all quarkonium states except the ground state bottomonium dissolve in the quark gluon plasma [93]. The upper limits on the dissociation temperatures for different quarkonium states obtained in this analysis are given in Table 6.

state	$\chi_c$	$\psi'$	$J/\psi$	$\Upsilon'$	$\chi_b$	$\Upsilon$
$T_{dis}$	$\leq T_c$	$\leq T_c$	$1.2T_c$	$1.2T_c$	$1.3T_c$	$2T_c$

Table 2. Upper bound on the dissociation temperatures for different quarkonium states in 2+1 flavor QCD [93].

## 7. Conclusion

In this paper we discussed quarkonium properties in quark gluon plasma. We discussed how color screening can be studied non-perturbatively on the lattice using spatial correlation functions of static quark and anti-quark. We discussed the importance of singlet and adjoint (triplet for  $SU(2)$  or octet for  $SU(3)$ ) degrees of freedom for understanding the temperature dependence of static meson (quark-antiquark) correlators. It has been shown how color singlet and adjoint degrees of freedom can be defined in the effective field theory framework, the so-called thermal pNRQCD.

We have seen that the singlet correlators of static quark and anti-quark show strong screening effects at distances comparable to quarkonium size. Thus it is nat-

ural to expect that most quarkonium states melt in quark gluon plasma. Quite surprisingly lattice calculations of quarkonium correlators in Euclidean time show very little temperature dependence. We reviewed the current status of these calculations in quenched QCD. It turns out that the spatial lattice spacing should be smaller than  $(4\text{GeV})^{-1}$  to have full control over the discretization errors. Therefore the extension of these calculations to full QCD pioneered in Ref. [94] will be quite difficult.

The only source of significant temperature dependence of quarkonium correlators is the zero mode contribution which is not related to bound states but to transport properties of heavy quarks in the medium [81]. We have shown that this contribution can be well described by a quasi-particle model with temperature dependent heavy quark mass. We have presented the calculations of quarkonium spectral functions in potential model and have shown that all quarkonium states, except the ground state bottomonium melt in the deconfined phase. We have also shown how the seemingly existing contradiction of strong color screening leading to quarkonium melting and very weak temperature dependence of quarkonium correlators can be resolved within potential models. It turns out that strong threshold enhancement of quarkonium spectral functions can compensate the absence of bound state and result in Euclidean correlators, which are almost temperature independent.

The fact that no charmonium bound states can exist in quark gluon plasma has important consequences for describing charmonium production in heavy ion collisions. In absence of bound states heavy quarks in the plasma can be treated quasi-classically using Langevin dynamics. In this scenario the residual correlation between the heavy quark and anti-quark, visible in the threshold enhancement and the finite life time of the plasma play an important role [95]. It turns out that using these ideas and the interactions of heavy quark determined in lattice QCD it is possible to understand the  $J/\psi$  suppression pattern at RHIC [95].

## Acknowledgements

This work was supported by U.S. Department of Energy under Contract No. DE-AC02-98CH10886. The work of A.B. was supported by grants DOE DE-FC02-06ER-41439 and NSF 0555397. A.V. work was supported by the Joint Theory Institute funded together by Argonne National Laboratory and the University of Chicago, and in part by the U.S. Department of Energy, Division of High Energy Physics and Office of Nuclear Physics, under Contract DE-AC02-06CH11357.

## References

- [1] T. Matsui and H. Satz,  $J/\psi$  Suppression by Quark-Gluon Plasma Formation, *Phys. Lett.* **B178**, 416, (1986).
- [2] A. Mocsy, Potential Models for Quarkonia. (2008), eprint 0811.0337 [hep-ph].
- [3] N. Brambilla, J. Ghiglieri, A. Vairo, and P. Petreczky, Static quark-antiquark pairs at finite temperature, *Phys. Rev.* **D78**, 014017, (2008).

- [4] N. Brambilla et al., Heavy quarkonium physics. (2004), eprint hep-ph/0412158.
- [5] N. Brambilla, A. Pineda, J. Soto, and A. Vairo, Effective field theories for heavy quarkonium, *Rev. Mod. Phys.* **77**, 1423, (2005).
- [6] W. E. Caswell and G. P. Lepage, Effective Lagrangians for Bound State Problems in QED, QCD, and Other Field Theories, *Phys. Lett.* **B167**, 437, (1986).
- [7] P. Petreczky, Heavy quark potentials and quarkonia binding, *Eur. Phys. J.* **C43**, 51–57, (2005).
- [8] M. Laine, O. Philipsen, P. Romatschke, and M. Tassler, Real-time static potential in hot QCD, *JHEP.* **03**, 054, (2007).
- [9] R. D. Pisarski, Damping rates for moving particles in hot QCD, *Phys. Rev.* **D47**, 5589–5600, (1993).
- [10] A. Beraudo, J. P. Blaizot, and C. Ratti, Real and imaginary-time  $Q\bar{Q}$  correlators in a thermal medium, *Nucl. Phys.* **A806**, 312–338, (2008).
- [11] K. G. Wilson, Confinement of quarks, *Phys. Rev.* **D10**, 2445–2459, (1974).
- [12] M. Albanese et al., Glueball Masses and String Tension in Lattice QCD, *Phys. Lett.* **B192**, 163, (1987).
- [13] M. Laine, O. Philipsen, and M. Tassler, Thermal imaginary part of a real-time static potential from classical lattice gauge theory simulations, *JHEP.* **09**, 066, (2007).
- [14] Y. Burnier, M. Laine, and M. Vepsäläinen, Heavy quarkonium in any channel in resummed hot QCD, *JHEP.* **01**, 043, (2008).
- [15] L. D. McLerran and B. Svetitsky, Quark Liberation at High Temperature: A Monte Carlo Study of SU(2) Gauge Theory, *Phys. Rev.* **D24**, 450, (1981).
- [16] S. Nadkarni, Nonabelian Debye Screening. 1. The Color Averaged Potential, *Phys. Rev.* **D33**, 3738, (1986).
- [17] P. Petreczky et al., Lattice calculation of medium effects at short and long distances, *Nucl. Phys.* **A698**, 400–403, (2002).
- [18] S. Digal, S. Fortunato, and P. Petreczky, Heavy quark free energies and screening in SU(2) gauge theory, *Phys. Rev.* **D68**, 034008, (2003).
- [19] O. Jahn and O. Philipsen, The Polyakov loop and its relation to static quark potentials and free energies, *Phys. Rev.* **D70**, 074504, (2004).
- [20] G. S. Bali, QCD forces and heavy quark bound states, *Phys. Rept.* **343**, 1–136, (2001).
- [21] C. J. Morningstar, K. J. Juge, and J. Kuti, Where is the string limit in QCD?, *Nucl. Phys. Proc. Suppl.* **73**, 590–595, (1999).
- [22] K. J. Juge, J. Kuti, and C. Morningstar, Fine structure of the QCD string spectrum, *Phys. Rev. Lett.* **90**, 161601, (2003).
- [23] C. Michael and S. J. Perantonis, Potentials and glueballs at large beta in SU(2) pure gauge theory, *J. Phys.* **G18**, 1725–1736, (1992).
- [24] N. Brambilla, A. Pineda, J. Soto, and A. Vairo, Potential NRQCD: An effective theory for heavy quarkonium, *Nucl. Phys.* **B566**, 275, (2000).
- [25] G. S. Bali and A. Pineda, QCD phenomenology of static sources and gluonic excitations at short distances, *Phys. Rev.* **D69**, 094001, (2004).
- [26] O. Kaczmarek, F. Karsch, E. Laermann, and M. Lutgemeier, Heavy quark potentials in quenched QCD at high temperature, *Phys. Rev.* **D62**, 034021, (2000).
- [27] S. Digal, P. Petreczky, and H. Satz, String breaking and quarkonium dissociation at finite temperatures, *Phys. Lett.* **B514**, 57–62, (2001).
- [28] S. Digal, P. Petreczky, and H. Satz, Quarkonium feed-down and sequential suppression, *Phys. Rev.* **D64**, 094015, (2001).
- [29] O. Kaczmarek, F. Karsch, P. Petreczky, and F. Zantow, Heavy Quark Anti-Quark Free Energy and the Renormalized Polyakov Loop, *Phys. Lett.* **B543**, 41–47, (2002).
- [30] O. Philipsen, Non-perturbative formulation of the static color octet potential, *Phys.*

- Lett.* **B535**, 138–144, (2002).
- [31] O. Kaczmarek, F. Karsch, P. Petreczky, and F. Zantow, Heavy quark free energies, potentials and the renormalized Polyakov loop, *Nucl. Phys. Proc. Suppl.* **129**, 560–562, (2004).
  - [32] O. Kaczmarek, F. Karsch, F. Zantow, and P. Petreczky, Static quark anti-quark free energy and the running coupling at finite temperature, *Phys. Rev.* **D70**, 074505, (2004).
  - [33] P. Petreczky and K. Petrov, Free energy of a static quark anti-quark pair and the renormalized Polyakov loop in three flavor QCD, *Phys. Rev.* **D70**, 054503, (2004).
  - [34] O. Kaczmarek and F. Zantow, Static quark anti-quark interactions in zero and finite temperature QCD. I: Heavy quark free energies, running coupling and quarkonium binding, *Phys. Rev.* **D71**, 114510, (2005).
  - [35] O. Kaczmarek, Screening at finite temperature and density, *PoS.* **CPOD07**, 043, (2007).
  - [36] RBC Collaboration. Work in progress.
  - [37] S. Necco and R. Sommer, The  $N(f) = 0$  heavy quark potential from short to intermediate distances, *Nucl. Phys.* **B622**, 328–346, (2002).
  - [38] R. Sommer, A New way to set the energy scale in lattice gauge theories and its applications to the static force and alpha-s in SU(2) Yang-Mills theory, *Nucl. Phys.* **B411**, 839–854, (1994).
  - [39] M. Cheng et al., The QCD Equation of State with almost Physical Quark Masses, *Phys. Rev.* **D77**, 014511, (2008).
  - [40] M. Luscher and P. Weisz, Locality and exponential error reduction in numerical lattice gauge theory, *JHEP.* **09**, 010, (2001).
  - [41] A. Bazavov, P. Petreczky, and A. Velytsky, Static quark anti-quark pair in SU(2) gauge theory, *Phys. Rev.* **D78**, 114026, (2008).
  - [42] S. P. Booth et al., Towards the continuum limit of SU(2) lattice gauge theory, *Phys. Lett.* **B275**, 424–428, (1992).
  - [43] G. P. Lepage and P. B. Mackenzie, On the viability of lattice perturbation theory, *Phys. Rev.* **D48**, 2250–2264, (1993).
  - [44] A. K. Rebhan, The NonAbelian Debye mass at next-to-leading order, *Phys. Rev.* **D48**, 3967–3970, (1993).
  - [45] A. K. Rebhan, NonAbelian Debye screening in one loop resummed perturbation theory, *Nucl. Phys.* **B430**, 319–344, (1994).
  - [46] A. Vairo, private communication . (2008).
  - [47] M. Le Bellac, *Thermal field theory*. Cambridge monographs on mathematical physics, (Cambridge Univ. Press, Cambridge, 1996).
  - [48] E. Braaten, R. D. Pisarski, and T.-C. Yuan, Production of soft dileptons in the quark-gluon plasma, *Phys. Rev. Lett.* **64**, 2242, (1990).
  - [49] A. Mocsy and P. Petreczky, Quarkonia correlators above deconfinement, *Phys. Rev.* **D73**, 074007, (2006).
  - [50] F. Karsch, E. Laermann, P. Petreczky, and S. Stickan, Infinite temperature limit of meson spectral functions calculated on the lattice, *Phys. Rev.* **D68**, 014504, (2003).
  - [51] G. Aarts and J. M. Martinez Resco, Continuum and lattice meson spectral functions at nonzero momentum and high temperature, *Nucl. Phys.* **B726**, 93–108, (2005).
  - [52] T. Umeda, K. Nomura, and H. Matsufuru, Charmonium at finite temperature in quenched lattice QCD, *Eur. Phys. J.* **C39S1**, 9–26, (2005).
  - [53] S. Datta, F. Karsch, P. Petreczky, and I. Wetzorke, Behavior of charmonium systems after deconfinement, *Phys. Rev.* **D69**, 094507, (2004).
  - [54] M. Asakawa and T. Hatsuda, Jpsi and etac in the deconfined plasma from lattice



- QCD, *Phys. Rev. Lett.* **92**, 012001, (2004).
- [55] A. Jakovac, P. Petreczky, K. Petrov, and A. Velytsky, Quarkonium correlators and spectral functions at zero and finite temperature, *Phys. Rev.* **D75**, 014506, (2007).
  - [56] T. R. Klassen, The anisotropic Wilson gauge action, *Nucl. Phys.* **B533**, 557–575, (1998).
  - [57] P. Chen, Heavy quarks on anisotropic lattices: The charmonium spectrum, *Phys. Rev.* **D64**, 034509, (2001).
  - [58] A. X. El-Khadra, A. S. Kronfeld, and P. B. Mackenzie, Massive Fermions in Lattice Gauge Theory, *Phys. Rev.* **D55**, 3933–3957, (1997).
  - [59] R. G. Edwards, U. M. Heller, and T. R. Klassen. unpublished. (1999).
  - [60] M. Okamoto et al., Charmonium Spectrum from Quenched Anisotropic Lattice QCD, *Phys. Rev.* **D65**, 094508, (2002).
  - [61] A. Gray et al., The Upsilon spectrum and  $m_b$  from full lattice QCD, *Phys. Rev.* **D72**, 094507, (2005).
  - [62] S. Datta, F. Karsch, P. Petreczky, and I. Wetzorke, A study of charmonium systems across the deconfinement transition, *Nucl. Phys. Proc. Suppl.* **119**, 487–489, (2003).
  - [63] S. Datta, F. Karsch, S. Wissel, P. Petreczky, and I. Wetzorke, Charmonia at finite momenta in a deconfined plasma. (2004), eprint hep-lat/0409147.
  - [64] P. Petreczky, On temperature dependence of quarkonium correlators. (2008), eprint 0810.0258 [hep-lat].
  - [65] M. Asakawa, T. Hatsuda, and Y. Nakahara, Maximum entropy analysis of the spectral functions in lattice QCD, *Prog. Part. Nucl. Phys.* **46**, 459–508, (2001).
  - [66] G. P. Lepage et al., Constrained curve fitting, *Nucl. Phys. Proc. Suppl.* **106**, 12–20, (2002).
  - [67] R. K. Bryan, Maximum entropy analysis of oversampled data problems, *Eur. Biophys. J.* **18**, 165–174, (1990).
  - [68] Y. Nakahara, M. Asakawa, and T. Hatsuda, Hadronic spectral functions in lattice QCD, *Phys. Rev.* **D60**, 091503, (1999).
  - [69] T. Yamazaki et al., Spectral function and excited states in lattice QCD with maximum entropy method, *Phys. Rev.* **D65**, 014501, (2002).
  - [70] F. Karsch, E. Laermann, P. Petreczky, S. Stickan, and I. Wetzorke, A lattice calculation of thermal dilepton rates, *Phys. Lett.* **B530**, 147–152, (2002).
  - [71] F. Karsch et al., Hadron correlators, spectral functions and thermal dilepton rates from lattice QCD, *Nucl. Phys.* **A715**, 701–704, (2003).
  - [72] M. Asakawa, T. Hatsuda, and Y. Nakahara, Hadronic spectral functions above the QCD phase transition, *Nucl. Phys.* **A715**, 863–866, (2003).
  - [73] T. Blum and P. Petreczky, Cutoff effects in meson spectral functions, *Nucl. Phys. Proc. Suppl.* **140**, 553–555, (2005).
  - [74] P. Petreczky, Lattice calculations of meson correlators and spectral functions at finite temperature, *J. Phys.* **G30**, S431–S440, (2004).
  - [75] P. Petreczky, F. Karsch, E. Laermann, S. Stickan, and I. Wetzorke, Temporal quark and gluon propagators: Measuring the quasiparticle masses, *Nucl. Phys. Proc. Suppl.* **106**, 513–515, (2002).
  - [76] C. R. Allton, J. E. Clowser, S. J. Hands, J. B. Kogut, and C. G. Strouthos, Application of the maximum entropy method to the (2+1)d four-fermion model, *Phys. Rev.* **D66**, 094511, (2002).
  - [77] K. Langfeld, H. Reinhardt, and J. Gattnar, Gluon propagators and quark confinement, *Nucl. Phys.* **B621**, 131–156, (2002).
  - [78] H. R. Fiebig, Spectral density analysis of time correlation functions in lattice QCD using the maximum entropy method, *Phys. Rev.* **D65**, 094512, (2002).

- [79] K. Sasaki, S. Sasaki, and T. Hatsuda, Spectral analysis of excited nucleons in lattice QCD with maximum entropy method, *Phys. Lett.* **B623**, 208–217, (2005).
- [80] T. Umeda, A constant contribution in meson correlators at finite temperature, *Phys. Rev.* **D75**, 094502, (2007).
- [81] P. Petreczky and D. Teaney, Heavy quark diffusion from the lattice, *Phys. Rev.* **D73**, 014508, (2006).
- [82] C. T. H. Davies et al., Precision Upsilon spectroscopy from nonrelativistic lattice QCD, *Phys. Rev.* **D50**, 6963–6977, (1994).
- [83] X. Liao and T. Manke, Relativistic bottomonium spectrum from anisotropic lattices, *Phys. Rev.* **D65**, 074508, (2002).
- [84] S. Datta, A. Jakovac, F. Karsch, and P. Petreczky, Quarkonia in a deconfined gluonic plasma, *AIP Conf. Proc.* **842**, 35–37, (2006).
- [85] A. Mocsy and P. Petreczky, Can quarkonia survive deconfinement?, *Phys. Rev.* **D77**, 014501, (2008).
- [86] M. Laine, A resummed perturbative estimate for the quarkonium spectral function in hot QCD, *JHEP.* **05**, 028, (2007).
- [87] A. Mocsy and P. Petreczky, Describing Charmonium Correlation Functions in Euclidean Time, *Eur. Phys. J. ST.* **155**, 101–106, (2008).
- [88] A. Mocsy and P. Petreczky, Heavy quarkonia survival in potential model, *Eur. Phys. J.* **C43**, 77–80, (2005).
- [89] W. M. Alberico, A. Beraudo, A. De Pace, and A. Molinari, Potential models and lattice correlators for quarkonia at finite temperature, *Phys. Rev.* **D77**, 017502, (2008).
- [90] D. Cabrera and R. Rapp, T-matrix approach to quarkonium correlation functions in the QGP, *Phys. Rev.* **D76**, 114506, (2007).
- [91] H. T. Ding, O. Kaczmarek, F. Karsch, and H. Satz, Charmonium correlators and spectral functions at finite temperature. (2009), eprint 0901.3023 [hep-lat].
- [92] Y. Burnier, M. Laine, and M. Vepsalainen, Heavy quark medium polarization at next-to-leading order, *JHEP.* **02**, 008, (2009).
- [93] A. Mocsy and P. Petreczky, Color Screening Melts Quarkonium, *Phys. Rev. Lett.* **99**, 211602, (2007).
- [94] G. Aarts, C. Allton, M. B. Oktay, M. Peardon, and J.-I. Skullerud, Charmonium at high temperature in two-flavor QCD, *Phys. Rev.* **D76**, 094513, (2007).
- [95] C. Young and E. Shuryak, Charmonium in strongly coupled quark-gluon plasma. (2008), eprint 0803.2866 [nucl-th].